

NNLO event generation for $pp \rightarrow Zh \rightarrow \ell^+ \ell^- b\bar{b}$ production in the SM effective field theory

Ulrich Haisch,¹ Darren J. Scott,¹ Marius Wieseemann,¹ Giulia Zanderighi^{1,2}
and Silvia Zanoli¹

¹*Max Planck Institute for Physics,
Föhringer Ring 6, 80805 München, Germany*

²*Physik-Department, Technische Universität München,
James-Frank-Strasse 1, 85748 Garching, Germany*

E-mail: haisch@mpp.mpg.de, dscott@mpp.mpg.de,
marius.wieseemann@mpp.mpg.de, zanderi@mpp.mpg.de, zanoli@mpp.mpg.de

ABSTRACT: We consider associated Zh production with $Z \rightarrow \ell^+ \ell^-$ and $h \rightarrow b\bar{b}$ decays in hadronic collisions. In the framework of the Standard Model effective field theory (SMEFT) we calculate the QCD corrections to this process and achieve next-to-next-to-leading order plus parton shower (NNLO+PS) accuracy using the MiNNLO_{PS} method. This precision is obtained for a subset of six SMEFT operators, including the corrections from effective Yukawa- and chromomagnetic dipole-type interactions. Missing higher-order QCD effects associated with the considered dimension-six operators are estimated to have a relative numerical impact of less than a percent on the total rate once existing experimental limits on the relevant Wilson coefficients are taken into account. We provide a dedicated Monte Carlo (MC) code that evaluates the NNLO SMEFT corrections on-the-fly in the event generation. This MC generator is used to study the numerical impact of NNLO+PS corrections on the kinematic distributions in $pp \rightarrow Zh \rightarrow \ell^+ \ell^- b\bar{b}$ production employing simple SMEFT benchmark scenarios. We identify the invariant mass $m_{b\bar{b}}$ of the two b -tagged jets as well as the three-invariant jet mass $m_{b\bar{b}j}$ as particularly interesting observables to study SMEFT effects. These distributions receive contributions that change both their normalisation and shape with the latter modifications depending on the exact jet definition. To our knowledge SMEFT effects of this type have so far not been discussed in the literature. The presented MC generator can also serve as a starting point to obtain NNLO+PS accuracy for a suitable enlarged set of effective operators in the future.

Contents

1	Introduction	1
2	Preliminaries	3
3	Calculation in a nutshell	4
3.1	Factorisable contributions to the $h \rightarrow b\bar{b}$ decay	4
3.2	Non-factorisable contributions to the $h \rightarrow b\bar{b}$ decay	5
3.3	Contributions to $pp \rightarrow Zh$	8
3.4	NNLO+PS calculation and MC implementation	9
4	Phenomenological analysis	12
4.1	Inclusive $h \rightarrow b\bar{b}$ decay in the SMEFT	13
4.2	Differential $pp \rightarrow Zh \rightarrow \ell^+\ell^-b\bar{b}$ cross section in the SMEFT	14
5	Conclusions	18
A	Squared matrix elements	19
B	Numerical impact of C_{HG} and C_{3G}	23

1 Introduction

The Standard Model (SM) predicts that a Higgs boson with a mass of 125 GeV decays with a branching ratio close to 60% to a pair of bottom quarks. The most sensitive production channels for detecting $h \rightarrow b\bar{b}$ decays at the LHC are despite their notably smaller cross sections with respect to gluon-gluon fusion Higgs production, the associated production of a Higgs boson with a W or Z boson (Vh), where the leptonic decay of the vector boson enables a clean selection. The $h \rightarrow b\bar{b}$ decay mode has been observed by both the ATLAS and the CMS collaboration in LHC Run II [1, 2], and these measurements constrain the $h \rightarrow b\bar{b}$ signal strength in Vh production ($\mu_{b\bar{b}}^{Vh}$) to be SM-like within about 25%, at the level of one standard deviation. With ATLAS and CMS being able to collect new data very soon in LHC Run III and with the high-luminosity upgrade (HL-LHC) on the horizon, the precision of the $\mu_{b\bar{b}}^{Vh}$ measurements will improve significantly with an ultimate projected HL-LHC accuracy of 15% (5%) in the case of Wh (Zh) production [3, 4].

Future LHC measurements of in particular $pp \rightarrow Zh \rightarrow \ell^+\ell^-b\bar{b}$ production will thus allow to place strong constraints on non-standard Higgs interactions. Assuming that any potential beyond-the-SM (BSM) contributions arises only from particles with masses much heavier than the electroweak (EW) scale, the SM effective field theory (SMEFT) [5–7] offers

a largely model-independent, systematically improvable quantum-field theoretical framework for analyses of BSM effects in collider processes that can be used to probe Higgs production and decay. In fact, radiative corrections in the SMEFT to both Vh production [8–10] and the $h \rightarrow f\bar{f}$ decays [11–14] have been calculated. The recent paper [15] has furthermore studied QCD corrections to $pp \rightarrow Zh \rightarrow \ell^+\ell^-\bar{b}\bar{b}$ in the anomalous-coupling framework (see also [16, 17] for earlier works on $pp \rightarrow Vh$ production in this context). The existing studies for Vh production have focused on the subset of higher-dimensional interactions that modify the couplings of the Higgs to EW gauge bosons achieving next-to-leading order (NLO) [8–10, 16, 17] and next-to-next-to-leading order (NNLO) [15] in QCD perturbation theory, respectively, while in the case of $h \rightarrow b\bar{b}$ both NLO QCD and NLO EW corrections to the total decay width have been calculated for the full set of relevant dimension-six SMEFT operators [11–13].

The ultimate goal of a SMEFT calculation of the $pp \rightarrow Zh \rightarrow \ell^+\ell^-\bar{b}\bar{b}$ process consists in taking into account all relevant contributions of dimension-six operators to both $pp \rightarrow Zh$ and $h \rightarrow b\bar{b}$, and to combine the production and the decay processes into a Monte Carlo (MC) event generator that consistently includes higher-order QCD and EW corrections at fixed order as well as parton-shower (PS) effects. Within the SM such computations have reached NNLO+PS precision [18–21], which means that they include NNLO QCD corrections to $pp \rightarrow Zh \rightarrow \ell^+\ell^-\bar{b}\bar{b}$ production as well as the matching to PS MC generators. A dedicated PS MC code including both NLO QCD and EW corrections within the SM also exists [22].

The intent of this work is to achieve NNLO+PS accuracy in the SMEFT including all dimension-six operator insertions that contribute to the subprocesses $pp \rightarrow Zh$ and $h \rightarrow b\bar{b}$ directly in QCD. This requires to calculate QCD corrections for a subset of six SMEFT operators, including effects associated to effective Yukawa- and chromomagnetic dipole-type interactions. The inclusion of these contributions in the NNLO+PS event generation yields an accurate description of the SMEFT effects in differential predictions for the full $pp \rightarrow Zh \rightarrow \ell^+\ell^-\bar{b}\bar{b}$ reaction. Since the distribution of the invariant mass $m_{b\bar{b}}$ of the two b -tagged jets (b -jets) receives contributions that change both its normalisation and shape it turns out to provide a particularly useful observable in the context of the SMEFT. The latter modifications depend on the b -jet definition, a feature that has not been discussed in the SMEFT literature as far as we know. Similar observations can be made for the three-jet invariant mass $m_{b\bar{b}j}$. As a by-product of our computations we are also able to extend the calculation of the inclusive $h \rightarrow b\bar{b}$ decay rate in the SMEFT [12] to the next order in QCD for the case that bottom quarks are treated as massless. On the other hand, non-trivial EW corrections arising in the SMEFT, such as a modified hZZ coupling, are not taken into account in our analysis. Since QCD and EW SMEFT corrections to $pp \rightarrow Zh \rightarrow \ell^+\ell^-\bar{b}\bar{b}$ approximately factorise, in the sense that the EW operators contributing to production play only a subleading role in the decay and vice versa, obtaining NNLO+PS accuracy for a suitable enlarged set of effective operators should be rather straightforward. While beyond the scope of this publication, we plan to return to this problem in the future.

This manuscript is structured as follows: in Section 2 we specify the subset of dimension-six operators of the full SMEFT Lagrangian that are relevant in the context of this arti-

cle, including a discussion of the normalisation chosen for the individual effective interactions. Section 3 contains a brief description of the basic ingredients of the SMEFT calculations for $pp \rightarrow Zh$ and $h \rightarrow b\bar{b}$ and their combination and implementation in our NNLO+PS event generator. The impact of the SMEFT corrections on kinematic distributions in $pp \rightarrow Zh \rightarrow \ell^+ \ell^- b\bar{b}$ production at NNLO+PS is presented in Section 4 by using simple benchmark scenarios for the Wilson coefficients. We conclude and present an outlook in Section 5. The lengthy analytic expressions for the squared matrix elements that are relevant for our work are relegated to Appendix A, while Appendix B contains numerical estimates of higher-order QCD corrections associated to the subset of the SMEFT operators that are considered in this paper. The discussed corrections have been neglected in our phenomenological study because they all turn out to contribute less than a percent once existing experimental limits on the relevant Wilson coefficients are taken into account.

2 Preliminaries

In this article we consider the following set of dimension-six operators

$$\begin{aligned}
Q_{H\Box} &= (H^\dagger H) \Box (H^\dagger H), & Q_{HD} &= (H^\dagger D_\mu H)^* (H^\dagger D^\mu H), \\
Q_{bH} &= y_b (H^\dagger H) \bar{q}_L b_R H, & Q_{bG} &= \frac{g_s^3}{(4\pi)^2} y_b \bar{q}_L \sigma_{\mu\nu} T^a b_R H G^{a,\mu\nu}, \\
Q_{HG} &= \frac{g_s^2}{(4\pi)^2} (H^\dagger H) G_{\mu\nu}^a G^{a,\mu\nu}, & Q_{3G} &= \frac{g_s^3}{(4\pi)^2} f^{abc} G_\mu^{a,\nu} G_\nu^{b,\sigma} G_\sigma^{c,\mu},
\end{aligned} \tag{2.1}$$

which appear in the full SMEFT Lagrangian

$$\mathcal{L}_{\text{SMEFT}} \supset \sum_i \frac{C_i}{\Lambda^2} Q_i. \tag{2.2}$$

Here $\Box = \partial_\mu \partial^\mu$, $\sigma_{\mu\nu} = i/2(\gamma_\mu \gamma_\nu - \gamma_\nu \gamma_\mu)$ with γ_μ the usual Dirac matrices, H denotes the SM Higgs doublet, q_L is the left-handed third-generation quark doublet, b_R is the right-handed bottom-quark singlet, while $g_s = \sqrt{4\pi\alpha_s}$ and $G_{\mu\nu}^a$ denote the coupling constant and the field strength tensor of QCD, respectively. The definition of the covariant derivative is $D_\mu = \partial_\mu - ig_s G_\mu^a T^a$ with T^a being the $SU(3)$ generators and f^{abc} denote the fully antisymmetric QCD structure constants. The bottom-quark Yukawa coupling is defined as $y_b = \sqrt{2}\bar{m}_b/v$, with the $\overline{\text{MS}}$ bottom-quark mass \bar{m}_b and the Higgs vacuum expectation value (VEV) v , while Λ denotes the new-physics mass scale that suppresses the dimension-six operators Q_i entering (2.2) and C_i are the corresponding Wilson coefficients. Notice finally that in the case of Q_{bH} and Q_{bG} the sum over the hermitian conjugate in (2.1) is understood.

The normalisations of the dimension-six operators introduced in (2.1) deserve some additional comments. First, the two mixed-chirality operators Q_{bH} and Q_{bG} include a factor of y_b which serves as an order parameter and explicitly appears in a broad class of ultraviolet (UV) completions that match onto the set of operators in (2.1). See for example the discussions in [23, 24]. Second, the factors of g_s and $1/(4\pi)^2$ that arise in

the definition of Q_{bG} , Q_{HG} and Q_{3G} guarantee that the associated Wilson coefficients C_{bG} , C_{HG} and C_{3G} are expected to be of $\mathcal{O}(1)$ in all weakly-coupled UV-complete extensions of the SM with new degrees of freedom and masses in the ballpark of Λ .¹ Notice that in the operator basis that has been employed in the NLO QCD calculation of the inclusive $h \rightarrow b\bar{b}$ decay rate in the SMEFT [12] a different normalisation is chosen for the operators Q_{bH} , Q_{bG} and Q_{HG} . As a result, in this normalisation the corresponding Wilson coefficients are expected to be of size $C_{bH} = \mathcal{O}(y_b) = \mathcal{O}(10^{-2})$, $C_{bG} = \mathcal{O}(y_b \alpha_s / (4\pi)) = \mathcal{O}(10^{-4})$ and $C_{HG} = \mathcal{O}(\alpha_s / (4\pi)) = \mathcal{O}(10^{-2})$ in weakly-coupled BSM theories and not $C_i = \mathcal{O}(1)$ as in the operator basis (2.1). Our normalisation therefore has the merit that the suppression factors y_b and $\alpha_s / (4\pi)$ appear explicitly as order parameters which allows for a more explicit power counting in our SMEFT calculation of QCD corrections to the $pp \rightarrow Zh \rightarrow \ell^+ \ell^- b\bar{b}$ process.

3 Calculation in a nutshell

In this section, we describe the different ingredients of the calculation of the QCD corrections to the fully differential decay rate of $h \rightarrow b\bar{b}$ and the Zh production cross section in the SMEFT. Throughout this work, we use the five-flavour scheme and thus treat the bottom quark as massless both in the matrix elements and the phase-space integrals. The bottom-quark Yukawa coupling is however taken to be non-zero. The explicit expressions for the non-trivial $h \rightarrow b\bar{b}$ squared matrix elements can be found in Appendix A. Moreover, we assume minimal-flavour violation [25] and set the Cabibbo-Kobayashi-Maskawa matrix element V_{tb} to unity. After having discussed the anatomy of the SMEFT corrections to both $pp \rightarrow Zh$ production and the $h \rightarrow b\bar{b}$ decay, we briefly mention the employed NNLO+PS methods and explain how we apply them to the event generation of the $pp \rightarrow Zh \rightarrow \ell^+ \ell^- b\bar{b}$ process including SMEFT effects.

3.1 Factorisable contributions to the $h \rightarrow b\bar{b}$ decay

Since the operators $Q_{H\Box}$, Q_{HD} and Q_{bH} do not contain a gluon the associated SMEFT contributions factorise to all orders in α_s . As a result, the matrix elements proportional to the Wilson coefficients $C_{H\Box}$, C_{HD} and C_{bH} can be obtained from the massless NNLO calculation of the fully differential $h \rightarrow b\bar{b}$ decay rate within the SM [26–28] by the following simple replacement:

$$y_b^2 \rightarrow y_b^2 (1 + 2c_{\text{fac}}), \quad (3.1)$$

with

$$c_{\text{fac}} = c_{\text{kin}} - c_{bH}, \quad c_{\text{kin}} = \frac{v^2}{\Lambda^2} \left[C_{H\Box} - \frac{C_{HD}}{4} \right], \quad c_{bH} = \frac{v^2}{\Lambda^2} \text{Re}(C_{bH}). \quad (3.2)$$

Notice that the term c_{kin} arises from the canonical normalisation of the Higgs kinetic term in the presence of $Q_{H\Box}$ and Q_{HD} . The squared Higgs VEV entering (3.2) is related to

¹In the case of the operator Q_{bG} the corresponding Wilson coefficient can also be of $\mathcal{O}(g^2/g_s^2)$ with g a weak coupling which implies that C_{bG} is parametrically smaller than $\mathcal{O}(1)$. This happens when Q_{bG} is generated by a EW and not a strong loop in the UV theory.

the Fermi constant G_F extracted from muon decay via $v^2 = 1/(\sqrt{2}G_F)$. EW tree-level corrections appearing in the SMEFT that modify the relation between the VEV and the Fermi constant (see for example [7, 11]) are very small and hence neglected in our analysis. In practice, our implementation relies on the expressions for the squared matrix elements provided in [27] which also have been used in the publications [18, 20, 21] to obtain NNLO+PS predictions for $pp \rightarrow Zh \rightarrow \ell^+ \ell^- b\bar{b}$ production within the SM.

Given the simplicity of the replacement (3.1) it is straightforward to obtain an analytic result for the factorisable corrections to the inclusive $h \rightarrow b\bar{b}$ decay rate due to $Q_{H\Box}$, Q_{HD} and Q_{bH} up to NNLO in QCD. The leading-order (LO) expression for the partial Higgs boson decay width to massless bottom-quark pairs within the SM is given by

$$\Gamma(h \rightarrow b\bar{b})_{\text{SM}}^{\text{LO}} = \frac{3y_b^2 m_h}{16\pi}. \quad (3.3)$$

Using this expression the corresponding NNLO result takes the form [29–31]

$$\Gamma(h \rightarrow b\bar{b})_{\text{SM}}^{\text{NNLO}} = (1 + \Delta) \Gamma(h \rightarrow b\bar{b})_{\text{SM}}^{\text{LO}}, \quad \Delta = \frac{\alpha_s}{\pi} 5.67 + \left(\frac{\alpha_s}{\pi}\right)^2 29.15. \quad (3.4)$$

Here both the bottom-quark Yukawa coupling y_b and the strong coupling constant α_s are understood to be renormalised at the scale m_h and we have assumed five active quark flavours to obtain the numerical results for the expansion coefficients appearing in Δ . By means of the replacement (3.1) one then finds

$$\Gamma(h \rightarrow b\bar{b})_{\text{SMEFT}}^{\text{NNLO, fac}} = (1 + 2c_{\text{fac}}) \Gamma(h \rightarrow b\bar{b})_{\text{SM}}^{\text{NNLO}}, \quad (3.5)$$

where the expressions for c_{fac} and $\Gamma(h \rightarrow b\bar{b})_{\text{SM}}^{\text{NNLO}}$ have already been given in (3.2) and (3.4), respectively. Since in the limit of massless bottom quarks the inclusive $h \rightarrow b\bar{b}$ decay rate is known to $\mathcal{O}(\alpha_s^4)$ [32–34] an extension of (3.5) to N⁴LO in QCD would be possible. Such higher-order QCD corrections are included in eHDECAY [35, 36], which allows to calculate the factorisable SMEFT corrections to $h \rightarrow b\bar{b}$ in the so-called strongly-interacting light Higgs or SILH [23] basis of dimension-six operators. Since the aim of this paper is to consistently achieve NNLO+PS accuracy for the fully differential decay rate of $h \rightarrow b\bar{b}$ in the SMEFT, the result in (3.5) will however be sufficient for our purposes.

3.2 Non-factorisable contributions to the $h \rightarrow b\bar{b}$ decay

Insertions of the operator Q_{bG} lead to non-factorisable QCD corrections to the fully differential $h \rightarrow b\bar{b}$ decay rate. Examples of the respective Feynman diagrams are shown in Figure 1. The relevant squared matrix elements are found by interfering the SMEFT contributions with the corresponding SM amplitudes. The explicit expressions for the resulting squared matrix elements can be found in Appendix A. The leading contribution arises at $\mathcal{O}(y_b^2 \alpha_s^2 C_{bG})$ from the interference of the $h \rightarrow b\bar{b}g$ amplitude in the SMEFT (upper left diagram) and the corresponding SM graphs. Notice that this real contribution is IR finite and that the corresponding one-loop contribution to $h \rightarrow b\bar{b}$ is identical to zero since it only involves scaleless integrals. In the operator basis (2.1) the first non-factorisable QCD corrections involving the operator Q_{bG} therefore appear at NNLO in QCD. In terms

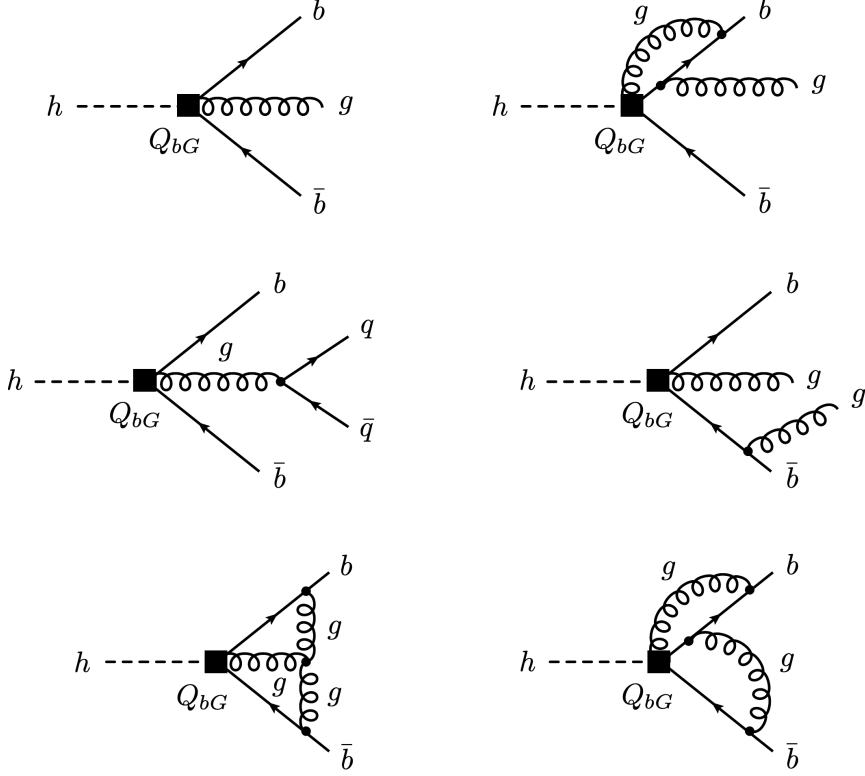


Figure 1: Examples of SMEFT contributions to the fully differential $h \rightarrow b\bar{b}$ decay rate involving an insertion of the operator Q_{bG} (black square). The upper left (right) diagram represents a tree-level (one-loop) contribution to the $h \rightarrow b\bar{b}g$ decay, the center left (right) diagram yields a tree-level contribution to the $h \rightarrow b\bar{b}q\bar{q}$ ($h \rightarrow b\bar{b}gg$) process, while the lower diagrams contribute to the $h \rightarrow b\bar{b}$ amplitude at the two-loop level. Notice that the quark flavours in the center left $h \rightarrow b\bar{b}q\bar{q}$ diagram can be $q = u, d, s, c, b$ and that effective five-point $hb\bar{b}gg$ vertices also contribute in the case of the $h \rightarrow b\bar{b}g$ transition. See text for further details.

of the inclusive LO SM decay rate (3.3), we find by integrating (A.1) over the three-particle phase space the following compact expression:

$$\Gamma(h \rightarrow b\bar{b})_{\text{SMEFT}}^{\text{NNLO,non}} = \Delta_{\text{non}} c_{bG} \Gamma(h \rightarrow b\bar{b})_{\text{SM}}^{\text{LO}}, \quad \Delta_{\text{non}} = \left(\frac{\alpha_s}{\pi}\right)^2 \frac{m_h^2}{3v^2}, \quad (3.6)$$

with

$$c_{bG} = \frac{v^2}{\Lambda^2} \text{Re}(C_{bG}). \quad (3.7)$$

We emphasise that when taking the difference in the normalisation of the operator Q_{bG} into account, the result (3.6) agrees with the expression derived in [12] after taking the limit $m_b \rightarrow 0$.

In Section 2 we have argued that the Wilson coefficient of Q_{bG} is expected to be of $\mathcal{O}(1)$ in a wide class of UV-complete theories if the operator is normalised as in (2.1). While there

are strong bounds on the imaginary part of C_{bG} from the electric dipole moment of the neutron [37], the real part entering (3.7) is at present only very weakly constrained by experiments [37–39]. In fact, values of $c_{bG} = \mathcal{O}(100)$ are compatible with all existing low- and high-energy data (see Section 4 for details), and therefore from a purely phenomenological point of view it is possible that $\alpha_s/\pi c_{bG} = \mathcal{O}(1)$ or even larger. In such a case the NNLO correction in (3.6) is numerically of the size of a NLO correction. To deal with this possibility we decided to include in our work also all contributions of $\mathcal{O}(y_b^2 \alpha_s^3 C_{bG})$. As shown in Figure 1 there are three types of such contributions. There are virtual (upper right diagram) or real corrections to the Born-level process $h \rightarrow b\bar{b}g$, the latter of which lead to either $h \rightarrow b\bar{b}q\bar{q}$ (center left diagram) or $h \rightarrow b\bar{b}gg$ (center right diagram). Notice that the four-quark final state involves the quark flavours $q = u, d, s, c, b$ and that final-state configurations with two bottom quarks and two gluons receive contributions from both effective $hb\bar{b}g$ and $hb\bar{b}gg$ vertices. Also the two-loop virtual corrections to the $h \rightarrow b\bar{b}$ decay (lower diagrams) contribute at $\mathcal{O}(y_b^2 \alpha_s^3 C_{bG})$. In Section 4 we will show that the inclusion of the N³LO corrections associated to Q_{bG} are phenomenologically relevant, which provides a further rationale to incorporate them in our NNLO+PS calculation of $pp \rightarrow Zh \rightarrow \ell^+ \ell^- b\bar{b}$ production.

We now turn our attention to the matrix elements involving the insertion of an operator Q_{HG} or Q_{3G} . In the former case one finds that in the limit of a massless bottom quark the operator Q_{HG} does not contribute to the $h \rightarrow b\bar{b}$ decay. This is related to the fact that for $m_b = 0$ an insertion of Q_{HG} does not lead to amplitudes such as $h \rightarrow b\bar{b}$ where the final-state bottom quarks have mixed chiralities. This feature is well-known from the SM calculation of the inclusive $h \rightarrow b\bar{b}$ rate where amplitudes involving a $h \rightarrow gg$ subdiagram first contribute at NNLO in QCD [40, 41] and only if non-zero quark masses are considered. In fact, the latter results receive Sudakov-like double logarithms of the form $\alpha_s^2 \ln^2(m_b^2/m_h^2)$ from both real and virtual contributions. The same feature is present in the SMEFT calculations of $h \rightarrow f\bar{f}$ processes [12–14]. While bottom-quark mass effects in the fully differential SM $h \rightarrow b\bar{b}$ decay rate have been studied at NNLO [42–45], it is not known how to resum the double-logarithmic contributions in the case of the $h \rightarrow b\bar{b}$ decay.² Likewise, it is also unknown how to correctly treat such terms in any of the existing NNLO+PS procedures. We therefore neglect all corrections associated to the insertion of Q_{HG} , which is formally correct in the limit of massless bottom quarks. We show in Appendix B that the corrections to the inclusive $\Gamma(h \rightarrow b\bar{b})$ decay rate proportional to C_{HG} and at leading power in m_b can be bounded in a model-independent fashion to the level of a few permille. Neglecting such effects in the calculation of the fully differential $\Gamma(h \rightarrow b\bar{b})$ decay rate can therefore also be assumed to be an excellent approximation.

Employing the operator basis introduced in (2.1) insertions of Q_{3G} induce tree-level corrections to $h \rightarrow b\bar{b}gg$ and one-loop corrections to $h \rightarrow b\bar{b}g$. After interfering these two types of contributions with the relevant SM amplitudes the resulting SMEFT corrections are proportional to $\mathcal{O}(y_b^2 \alpha_s^3 C_{3G})$ and hence formally of N³LO. Since our goal is it to only

²In the case of the inclusive $h \rightarrow \gamma\gamma$ and $h \rightarrow gg$ decays it has been shown how to resum the leading double-logarithmic corrections [46–49].

attain NNLO+PS precision we neglect corrections due to Q_{3G} . In Appendix B we present an estimate of this type of N³LO corrections that suggests that given the existing bounds on the Wilson coefficient C_{3G} , SMEFT contributions of $\mathcal{O}(y_b^2 \alpha_s^3 C_{3G})$ can indeed only have a very minor numerical impact on the $h \rightarrow b\bar{b}$ decay distributions.

3.3 Contributions to $pp \rightarrow Zh$ production

Let us first recall that the only effective dimension-six EW interactions that we are taking into account in our analysis are related to the three operators $Q_{H\Box}$, Q_{HD} and Q_{bH} introduced in (2.1) and that otherwise we only consider effective interactions that directly induce QCD corrections. In particular, dimension-six SMEFT operators that lead to non-trivial modifications of the hZZ vertex are not considered in our work.

With this simplification the dominant corrections to Zh production in the SMEFT are associated to $Q_{H\Box}$ and Q_{HD} . These operators already provide a contribution at Born level which can be obtained by the shift

$$g_{hZZ}^2 \rightarrow g_{hZZ}^2 (1 + 2c_{\text{kin}}), \quad (3.8)$$

where $g_{hZZ} = 2m_Z^2/v$ denotes the SM coupling between a Higgs and two Z bosons with m_Z the Z -boson mass. The coefficient c_{kin} has been defined in (3.2). Applying the rescaling (3.8) to the inclusive Zh production cross section in the SM one obtains the following formula

$$\sigma(pp \rightarrow Zh)_{\text{SMEFT}}^{\text{NNLO}} = (1 + 2c_{\text{kin}}) \sigma(pp \rightarrow Zh)_{\text{SM}}^{\text{NNLO}}, \quad (3.9)$$

for the SMEFT corrections to the cross section up to NNLO. An analogous expression also holds at the differential level.

Let us also discuss the role of operators other than $Q_{H\Box}$ and Q_{HD} in associated Higgs production with a vector boson. For massless bottom quarks neither Q_{bH} nor Q_{bG} furnishes a non-zero contribution to $pp \rightarrow Zh$ to all orders in the strong coupling constant α_s due to the mixed-chirality nature of the two operators. Insertions of Q_{HG} lead to a tree-level and an one-loop correction to $q\bar{q} \rightarrow Zhg$ and $q\bar{q} \rightarrow Zh$, respectively. After interfering these amplitudes with their SM counterparts one obtains a contribution that is of $\mathcal{O}(\alpha_s^2 C_{HG})$ with respect to the LO Zh production cross section within the SM. While these corrections are therefore formally needed to achieve NNLO+PS accuracy, we will show in Appendix B that the contributions proportional to C_{HG} cannot exceed the level of a few permille. This renders them irrelevant for all practical purposes and we hence neglect them. We note that by using the results of [50] their inclusion would be quite straightforward, but given their subleading impact we refrain from doing so. Finally, the operator Q_{3G} gives rise to tree-level (one-loop) corrections to $q\bar{q} \rightarrow Zhgg$ ($q\bar{q} \rightarrow Zhg$). Both contributions are of $\mathcal{O}(\alpha_s^3 C_{3G})$ and therefore we do not take them into account in our analysis. In Appendix B we nevertheless estimate their potential size and show them to be negligible for our purposes. We finally add that contributions to $gg \rightarrow Zh$ production, which is loop suppressed in the SM, do either vanish in the limit $m_b = 0$ as for Q_{bH} and Q_{bG} or are at least of $\mathcal{O}(\alpha_s^3)$ like in the case of Q_{HG} and Q_{3G} . Contributions to the $gg \rightarrow Zh$ process arising from (2.1) are therefore phenomenologically irrelevant.

3.4 NNLO+PS calculation and MC implementation

In the following, we discuss how the fixed-order QCD results including the set of dimension-six operators in (2.1) are implemented into the NNLO+PS accurate $h \rightarrow b\bar{b}$ generator developed in [20]. We then describe how the $h \rightarrow b\bar{b}$ decay events can be combined with Higgs production events from any Higgs production mode, including SMEFT effects consistently. While in this paper we consider the case of associated Zh production, the modifications to the formulae required for other processes are straightforward as long as one works in the narrow width approximation for the Higgs propagator.

We start our discussion by briefly recalling how NNLO+PS accurate results for the $h \rightarrow b\bar{b}$ decay can be achieved in the SM. The simplest way to obtain NNLO+PS precision is to compute decay events by applying the so-called MiNLO' method [51, 52]. The weights are then rescaled to the NNLO accurate inclusive $h \rightarrow b\bar{b}$ decay rate $\Gamma(h \rightarrow b\bar{b})_{\text{SM}}^{\text{NNLO}}$ by multiplying the event weights with the ratio $\Gamma(h \rightarrow b\bar{b})_{\text{SM}}^{\text{NNLO}}/\Gamma(h \rightarrow b\bar{b})_{\text{SM}}^{\text{MiNLO}'}$, where the denominator is directly computed from the MiNLO' events by summing their weights. As a variant, it is also possible to restrict the NNLO correction to a certain phase space region. In particular, one can use a rescaling factor that tends to one in the region where the decay events involve hard radiation, while requiring the integral of the rescaled events to reproduce exactly $\Gamma(h \rightarrow b\bar{b})_{\text{SM}}^{\text{NNLO}}$. In this work, we follow such an approach and specifically employ the procedure described in Section 2.2 of the article [20].

As discussed in Sections 3.1 and 3.2, the SMEFT corrections to $h \rightarrow b\bar{b}$ split into factorisable and non-factorisable corrections. The factorisable SMEFT effects can be taken into account by using an analogous reweighting to (3.5) and applying it to the NNLO+PS accurate $h \rightarrow b\bar{b}$ events, i.e. by computing $(1 + 2c_{\text{fac}})\Gamma(h \rightarrow b\bar{b})_{\text{SM}}^{\text{NNLO}}/\Gamma(h \rightarrow b\bar{b})_{\text{SM}}^{\text{MiNLO}'}$ when reweighting the MiNLO' events. As far as non-factorisable corrections are concerned, they are separately IR finite, as pointed out already before. In particular, the leading contribution including Q_{bG} is of $\mathcal{O}(\alpha_s^2)$ and contributes to the squared matrix element of $h \rightarrow b\bar{b}g$, cf. (A.1), which features no divergence when the gluon is unresolved and will be referred to as R hereafter. Hence, the integration over the three-body phase space is IR finite without the need to apply the MiNLO' method, at variance with the NNLO+PS calculation of the factorisable part. At $\mathcal{O}(\alpha_s^3)$ the one-loop virtual and real corrections to the $h \rightarrow b\bar{b}g$ process are included, just as in a standard POWHEG NLO+PS calculation [53, 54]. In the following, we will refer to these contributions as RV and RR, respectively. Since their sum is IR finite, these corrections yield a contribution to the inclusive $h \rightarrow b\bar{b}$ decay rate when integrated over the three- and four-body phase space, respectively, and added together. To deal with the soft and collinear singularities of the real contributions and to cancel the IR poles of the one-loop virtual corrections, cf. (A.4), we exploit the general implementation of the Frixione-Kunszt-Signer (FKS) subtraction [55, 56] within the POWHEG-BOX framework [57]. To this end, the full POWHEG-BOX machinery is used that automatically builds the soft and collinear counterterms and remnants, and also checks the behaviour in the soft and collinear limits of the real squared matrix elements against their soft and collinear approximations. Finally, also the two-loop virtual corrections to $h \rightarrow b\bar{b}$ including Q_{bG} contribute to the non-factorisable SMEFT effects at $\mathcal{O}(\alpha_s^3)$. These corrections, called VV in what follows,

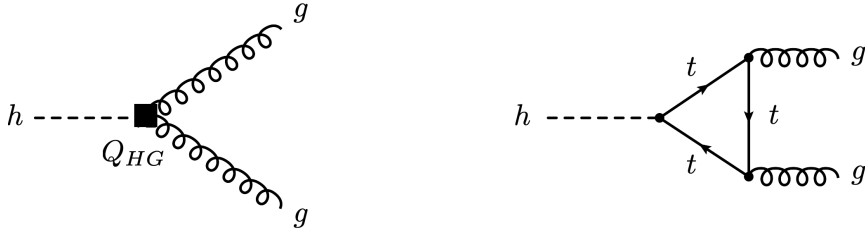


Figure 2: Illustration of the interference contribution that leads to the SMEFT correction proportional to c_{HG} in the partial decay width $h \rightarrow gg$ as given in (3.13). The left and right diagram represent the tree-level SMEFT with an Q_{HG} insertion (black square) and the one-loop SM contribution involving a top-quark loop, respectively. Light-quark loops also appear in the SM, but since these corrections vanish identically for $m_q = 0$, they turn out to be numerically insignificant and hence are ignored in our study.

are IR finite by themselves, cf. (A.18), and after integrating them over the two-particle phase space we find the compact expression

$$\Gamma(h \rightarrow b\bar{b})_{\text{SMEFT}}^{\text{non,VV}} = \frac{\alpha_s}{\pi} \frac{49}{12} \Delta_{\text{non}} c_{bG} \Gamma(h \rightarrow b\bar{b})_{\text{SM}}^{\text{LO}}, \quad (3.10)$$

with Δ_{non} and c_{bG} defined as in (3.6) and (3.7), respectively. The result in (3.10) can simply be added to the factorisable SMEFT contribution to the $h \rightarrow b\bar{b}$ decay.

To explain how we combine production and decay events in the SMEFT to obtain $pp \rightarrow Zh \rightarrow \ell^+ \ell^- b\bar{b}$ events, it is useful to first recall how such a combination can be achieved within the SM. In this case, the Higgs boson in each Zh production event is replaced by the possible decay products (i.e. $b\bar{b}g$, $b\bar{b}q\bar{q}$ or $b\bar{b}gg$) taken from a given decay event. Working in the narrow width approximation, the weight $w_{\text{full}}^{\text{SM}}$ of the full SM event is then calculated as

$$w_{\text{full}}^{\text{SM}} = \frac{w_{\text{prod}}^{\text{SM}} w_{\text{dec}}^{\text{SM}}}{\Gamma_h^{\text{SM}}}, \quad (3.11)$$

where $w_{\text{prod}}^{\text{SM}}$ denotes the weight of the production event obtained at NNLO+PS using the MiNNLO_{PS} $pp \rightarrow Zh$ generator presented in [21], while $w_{\text{dec}}^{\text{SM}}$ represents the weight of the decay event computed at NNLO+PS precision employing the MiNLO' method and procedure detailed in the work [20]. The total decay width Γ_h^{SM} of the 125 GeV SM Higgs boson serves as an input. The Les Houches event (LHE) file also stores, for each event, the value of the hardest radiation allowed by the shower (i.e. the scale `scalup`). We record in the combined LHE file the value of `scalupprod` for the production process and, once the event is passed to the PS, we recompute on-the-fly the value of `scalupdec` for the specific decay kinematics. We then generate emissions of the Higgs decay in all the available phase space and after the shower is complete we check whether the hardness of the splittings is below the veto scale `scalupdec`. If this is not the case we attempt to shower the event again until the condition is met. Additional details of this procedure are given in Section 3.2 of the paper [20].

From the above discussion one can deduce that NNLO+PS accurate differential cross sections for the full process $pp \rightarrow Zh \rightarrow \ell^+ \ell^- b\bar{b}$ in the SMEFT can be obtained by combining production and decay as follows

$$d\sigma_{\text{NNLO+PS}} = (1 + 2c_{\text{kin}})^2 \left\{ \left[1 - 2c_{bH} + \frac{\Gamma(h \rightarrow b\bar{b})_{\text{SMEFT}}^{\text{non,VV}}}{\Gamma(h \rightarrow b\bar{b})_{\text{SM}}^{\text{NNLO}}} \right] d\sigma_{\text{NNLO+PS}}^{\text{SM}} + d\sigma_{\text{NNLO+PS}}^{\text{non,R+RV+RR}} \right\} \frac{\Gamma_h^{\text{SM}}}{\Gamma_h^{\text{SMEFT}}}, \quad (3.12)$$

where we have factorised the term $(1 + 2c_{\text{kin}})^2$ that arises from the canonical normalisation of the Higgs kinetic term. The results for $\Gamma(h \rightarrow b\bar{b})_{\text{SM}}^{\text{NNLO}}$ and $\Gamma(h \rightarrow b\bar{b})_{\text{SMEFT}}^{\text{non,VV}}$ can be found in (3.4) and (3.10), $d\sigma_{\text{NNLO+PS}}^{\text{SM}}$ represents the NNLO+PS accurate differential cross section obtained interfacing the MiNNLO_{PS} calculation of the $pp \rightarrow Zh$ generator [21] with the reweighted MiNLO' calculation of the $h \rightarrow b\bar{b}$ generator [20], while $d\sigma_{\text{NNLO+PS}}^{\text{non,R+RV+RR}}$ includes the non-factorisable corrections R, RV and RR that we compute as discussed above. Notice that both $\Gamma(h \rightarrow b\bar{b})_{\text{SMEFT}}^{\text{non,VV}}$ and $d\sigma_{\text{NNLO+PS}}^{\text{non,R+RV+RR}}$ depend linearly on the Wilson coefficient c_{bG} . We stress that the advantage of expressing (3.12) in this form lies in the fact that arbitrary combinations of Wilson coefficients can be obtained without recalculating any of the individual cross sections. Thus, variations of the Wilson coefficients can be obtained a posteriori.

The last factor in (3.12) takes into account that the total decay width of the Higgs boson that appears in (3.11) is modified by SMEFT effects. In our implementation we employ the following result

$$\Gamma_h^{\text{SMEFT}} = (1 + 2c_{\text{kin}}) \left[\Gamma_h^{\text{SM}} - (2\Delta c_{bH} - K_{bG} \Delta_{\text{non}} c_{bG}) \Gamma(h \rightarrow b\bar{b})_{\text{SM}}^{\text{LO}} + 6K_{HG} c_{HG} \Gamma(h \rightarrow gg)_{\text{SM}}^{\text{LO}} \right]. \quad (3.13)$$

The LO expression for the partial decay width for $h \rightarrow b\bar{b}$ can be found in (3.3) and the corrections proportional to $\Gamma(h \rightarrow b\bar{b})_{\text{SM}}^{\text{LO}}$ have been included in (3.13) in the approximation that treats the bottom quark as strictly massless. The relevant correction factors Δ and Δ_{non} have been defined in (3.4) and (3.6), respectively. The multiplicative factor K_{bG} encodes the QCD corrections up to N³LO related to the Q_{bG} contribution to the partial decay width of $h \rightarrow b\bar{b}$. The used numerical value of $K_{bG} = 1.622$ follows from the semi-analytic formula given below in (4.3). The term in Γ_h^{SMEFT} proportional to

$$c_{HG} = \frac{v^2}{\Lambda^2} C_{HG}, \quad (3.14)$$

encodes the SMEFT corrections to the partial decay width of $h \rightarrow gg$ involving a single insertion of the operator Q_{HG} . The relevant diagrams are shown in Figure 2. These terms start at $\mathcal{O}(\alpha_s^2 C_{HG})$ since

$$\Gamma(h \rightarrow gg)_{\text{SM}}^{\text{LO}} = \frac{\alpha_s^2 m_h^3}{72\pi^3 v^2}. \quad (3.15)$$

This result holds in the limit of an infinite top-quark mass, which is a sufficiently accurate approximation for our purpose. To include higher-order effects proportional to C_{HG} in an approximate way we have incorporated the factor $K_{HG} = 1.844$ in (3.13). This K -factor includes QCD corrections up to N⁴LO [34]. Notice finally that (3.13) contains only QCD corrections related to the dimension-six SMEFT operators introduced in (2.1).³

We finally recall from the discussion in Section 3.3 that if one considers associated Zh production alone, the SMEFT production weight would be modified by a universal factor leading to

$$w_{\text{prod}}^{\text{SMEFT}} = (1 + 2c_{\text{kin}}) w_{\text{prod}}^{\text{SM}}. \quad (3.16)$$

The multiplicative factor $(1 + 2c_{\text{kin}})$, however, cancels against the same overall factor appearing in the total decay width of the Higgs boson when production and decay events are combined. This cancellation becomes manifest in (3.12) when (3.13) is used. If, on the other hand, one considers production processes other than $pp \rightarrow Zh$, where SMEFT effects give rise to non-universal corrections to the production process, some of the formulae given in this subsection need to be modified accordingly.

4 Phenomenological analysis

In the following we present NNLO+PS accurate results for $pp \rightarrow Zh \rightarrow \ell^+ \ell^- b \bar{b}$ production at the LHC with a centre-of-mass energy of $\sqrt{s} = 13 \text{ TeV}$ including the SMEFT effects discussed in Section 3. All SM input parameters are taken from the most recent PDG review [58]. In particular, we use $G_F = 1.166379 \cdot 10^{-5} \text{ GeV}^{-2}$, $m_Z = 91.1876 \text{ GeV}$, $\Gamma_Z^{\text{SM}} = 2.4952 \text{ GeV}$, $m_h = 125.09 \text{ GeV}$ and $\Gamma_h^{\text{SM}} = 4.1 \text{ MeV}$. The Higgs VEV is calculated using $v = 2^{-1/4} G_F^{-1/2} = 246.22 \text{ GeV}$, while the value of the electromagnetic coupling and the weak mixing angle is derived as $\alpha = \sqrt{2} G_F m_W^2 \sin^2 \theta_w / \pi = 1/132.184$ and $\sin^2 \theta_w = 1 - m_W^2 / m_Z^2 = 0.2230$ employing $m_W = 80.379 \text{ GeV}$. In the case of the bottom-quark mass we use the $\overline{\text{MS}}$ mass $\bar{m}_b(\bar{m}_b) = 4.18 \text{ GeV}$ as input which leads to $\bar{m}_b(m_h) = 2.79 \text{ GeV}$ and $y_b(m_h) = \sqrt{2} \bar{m}_b(m_h) / v = 1.60 \cdot 10^{-2}$. NNPDF31_nnlo_as_0118 parton distribution functions (PDFs) [59] with $\alpha_s(m_Z) = 0.1180$ giving rise to $\alpha_s(m_h) = 0.1127$ are employed in our MC simulations and events are showered with Pythia 8 [60] utilising the Monash tune [61]. Effects from hadronisation, underlying event modelling or QED effects in the shower are not included.

We study two SMEFT benchmark scenarios. In both cases we set the Wilson coefficients c_{kin} , c_{HG} and c_{3G} to zero — see (3.2) and (3.14). In the first scenario, we choose $c_{bH} \neq 0$ and $c_{bG} = 0$, while in the second one we take $c_{bH} = 0$ and $c_{bG} \neq 0$. Before specifying our benchmark settings for the two parameters, let us summarise the existing experimental constraints on c_{bH} and c_{bG} . In the former case, we take the result from a recent global SMEFT fit [62] that includes 34 dimension-six operators. In the normalisation of (2.1)

³By adding the term $\Delta \Gamma_h^{\text{SMEFT}} = -(1 + 2c_{\text{kin}}) \sum_{q=u,d,s,c} (2\Delta c_{qH} - K_{qG} \Delta_{\text{non}} c_{qG}) \Gamma(h \rightarrow q\bar{q})_{\text{SM}}^{\text{LO}}$ to (3.13) with $K_{qG} = 1.622$ it is straightforward to include the dominant SMEFT corrections to the partial decay widths for $h \rightarrow q\bar{q}$.

and (3.2), this work provides the following marginalised 95% confidence level (CL) bound

$$c_{bH} \in [-0.13, 0.20]. \quad (4.1)$$

In the case of c_{bG} one instead has

$$c_{bG} \in [-438, 438], \quad (4.2)$$

at 95% CL, which has been obtained in [37] from an analysis of the transverse momentum (p_T) spectrum of Z -boson production in association with b -jets as measured by ATLAS in LHC Run II [63]. We add that the nominal strongest bound on c_{bG} has been derived in [37] and relies on high-mass b -jet pair production ATLAS data [64]. While this search imposes $c_{bG} \in [-149, 149]$ it is not clear to which extent a SMEFT treatment is trustworthy in this high-mass region, so that we do not use it here. The present bounds from Higgs physics on the Wilson coefficient c_{bG} [38, 39] are weaker than the constraint given in (4.2).

4.1 Inclusive $h \rightarrow b\bar{b}$ decay in the SMEFT

As a first application of the calculations outlined in Section 3 we extend the results for the inclusive $h \rightarrow b\bar{b}$ decay width in the SMEFT presented in [12] to the N³LO level in QCD for massless bottom quarks. In terms of the LO SM inclusive decay width (3.3) we find

$$\begin{aligned} \Gamma(h \rightarrow b\bar{b})_{\text{SMEFT}}^{\text{N}^3\text{LO}} = & \left\{ (1 + 2c_{\text{fac}}) \left[1 + \frac{\alpha_s}{\pi} 5.67 + \left(\frac{\alpha_s}{\pi}\right)^2 29.15 + \left(\frac{\alpha_s}{\pi}\right)^3 41.76 \right] \right. \\ & \left. + \left(\frac{\alpha_s}{\pi}\right)^2 \frac{m_h^2}{3v^2} \left[1 + \frac{\alpha_s}{\pi} 17.32 \right] c_{bG} \right\} \Gamma(h \rightarrow b\bar{b})_{\text{SM}}^{\text{LO}}, \end{aligned} \quad (4.3)$$

if the renormalisation scale is identified with the Higgs boson mass by setting $\mu = m_h$. Notice that the $\mathcal{O}(\alpha_s^3)$ corrections proportional to $(1 + 2c_{\text{fac}})$ are known from the SM calculation of the $h \rightarrow b\bar{b}$ decay [32–34]. The result for the $\mathcal{O}(\alpha_s^3)$ correction proportional to c_{bG} is instead new and given here for the first time. Notice that the latter terms enhance the non-factorisable contribution due to Q_{bG} by around 60%, which provides a clear motivation to incorporate them in our NNLO+PS generator. The corrections associated with Q_{HG} and Q_{3G} are very small and not included in (4.3). See the discussion in Appendix B.

Using (4.3) one can now study the possible numerical impact of the set of dimension-six operators introduced in (2.1). Allowing for instance c_{bH} (c_{bG}) to vary within its experimentally allowed 95% CL range in eqs. (4.1) and (4.2), while setting all other Wilson coefficients to zero, leads to the following relative shifts in the inclusive $h \rightarrow b\bar{b}$ decay width:

$$\frac{\Gamma(h \rightarrow b\bar{b})_{\text{SMEFT}}^{\text{N}^3\text{LO}}}{\Gamma(h \rightarrow b\bar{b})_{\text{SM}}^{\text{N}^3\text{LO}}} - 1 \in \begin{cases} [-39, 26]\% & \text{for (4.1) and } c_{\text{kin}} = c_{bG} = 0, \\ [-6.3, 6.3]\% & \text{for (4.2) and } c_{\text{kin}} = c_{bH} = 0. \end{cases} \quad (4.4)$$

Thus, there is a hierarchy between the possible SMEFT effects in the $h \rightarrow b\bar{b}$ decay rate, with the non-factorisable contributions due to Q_{bG} being smaller by a factor of $\mathcal{O}(5)$ than the factorisable corrections that are associated to Q_{bH} (as well as $Q_{H\Box}$ and Q_{HD}).

The SMEFT QCD corrections in (B.3) and (B.7) due to Q_{HG} and Q_{3G} are smaller by more than a factor of $\mathcal{O}(20)$ compared to the contributions from Q_{bG} . Missing higher-order QCD effects in (4.3) can therefore only have a relative numerical impact of a few permille once existing experimental limits on the Wilson coefficients of the operators in (2.1) are taken into account.

4.2 Differential $pp \rightarrow Zh \rightarrow \ell^+ \ell^- b\bar{b}$ cross section in the SMEFT

In our differential analysis we select events with two charged leptons (electrons or muons) to explore the $Zh \rightarrow \ell^+ \ell^- b\bar{b}$ signature. The leptons are required to have a transverse momentum of $p_{T,\ell} > 15$ GeV and a pseudorapidity of $|\eta_\ell| < 2.5$. The invariant mass of the dilepton pair is restricted to $m_{\ell^+\ell^-} \in [75, 105]$ GeV. The events are furthermore required to have at least two b -jets, which are reconstructed using the anti- k_t algorithm [65] as implemented in `FastJet` [66]. We impose transverse momentum cuts of $p_{T,b} > 25$ GeV and a rapidity threshold of $|\eta_b| < 2.5$ on the b -jets. The definition of potential additional jets use the same thresholds as those of the b -jets. The dominant background processes are $Z + \text{jets}$, $t\bar{t}$, single-top and diboson production. The latter three types of backgrounds can be substantially reduced by requiring large values of $p_{T,Z}$ [67]. Hence, to improve the signal-to-background ratio we impose $p_{T,Z} \in [150, 250]$ GeV. Notice that this $p_{T,Z}$ requirement corresponds to the second resolved $p_{T,Z}$ bin as recommended in the stage 1.2 simplified template cross sections (STXS) framework [68–70] which is also implemented in the latest ATLAS LHC Run II measurements of the $pp \rightarrow Zh \rightarrow \ell^+ \ell^- b\bar{b}$ process [71, 72]. We will also comment on how our results are modified if the other two resolved regions, i.e. $p_{T,Z} \in [75, 150]$ GeV and $p_{T,Z} > 250$ GeV, are considered.

The two panels in Figure 3 display our predictions for the $pp \rightarrow Zh \rightarrow \ell^+ \ell^- b\bar{b}$ cross section differential in the invariant mass of the two b -jets, employing a jet radius of $R = 0.4$ in the anti- k_t clustering. If more than two b -jets are present the observable $m_{b\bar{b}}$ is defined as the invariant mass of the pair of b -jets closest to m_h . The black curves correspond to our SM NNLO+PS prediction for the 13 TeV LHC with central renormalisation scale μ_R and factorisation scale μ_F set according to the `MiNNLOPS` procedure [73, 74] and the gray band represents the corresponding perturbative uncertainties. These uncertainties have been obtained from seven-point scale variations enforcing the constraint $1/2 \leq \mu_R/\mu_F \leq 2$ and keeping the scale variation in production and decay correlated. The same way of estimating perturbative uncertainties is applied to all kinematic distributions that are provided in this section. The red histogram in the left and right panel of Figure 3 corresponds to the results for $c_{bH} = 0.15$ and $c_{bG} = 400$, respectively. These values are within the range allowed by (4.1) and (4.2). All other Wilson coefficients not specified in a given plot are set to zero.

From the left plot in Figure 3 it is evident that BSM effects in the form of a non-zero Wilson coefficient c_{bH} just lead to a rescaling of the $m_{b\bar{b}}$ spectrum. This is expected because c_{bH} is part of the factorisable corrections in (3.2) that just rescales all kinematic distributions by an overall factor. On the other hand, a non-zero Wilson coefficient c_{bG} is more interesting, since $c_{bG} \neq 0$ alters the shape of the $m_{b\bar{b}}$ distribution with respect to the SM prediction. This can be seen in the right panel of Figure 3. In fact, one observes that for the choices $c_{bG} = 400$ and $R = 0.4$ the $m_{b\bar{b}}$ spectrum receives relative corrections of up to

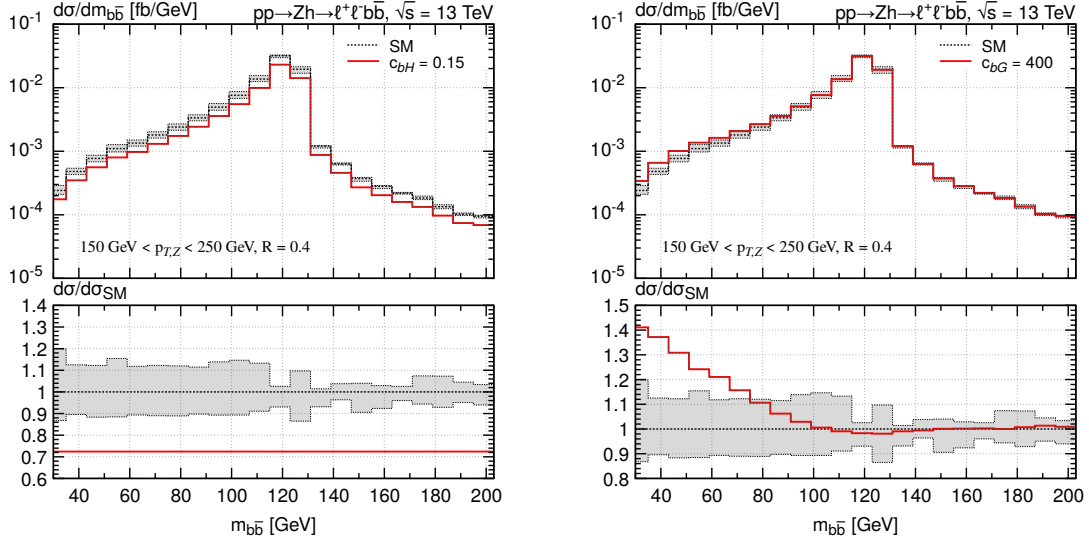


Figure 3: Invariant mass of the two b -jets using the anti- k_t algorithm with radius parameter $R = 0.4$. The red histogram in the left (right) panel corresponds to the prediction for $c_{bH} = 0.15$ ($c_{bG} = 400$). For comparison our SM prediction with its scale uncertainty band is shown in black and gray. All results correspond to proton-proton (pp) collisions at $\sqrt{s} = 13$ TeV and are subject to the fiducial cuts discussed in the main text. The lower panels depict the ratios between the BSM and the SM distributions.

40% for invariant masses $m_{b\bar{b}} \simeq 50$ GeV. The reason for this somewhat surprising feature is the structure of the tree-level squared matrix element, given in (A.1), that modifies the $h \rightarrow b\bar{b}g$ process and constitutes the leading Q_{bG} contribution. The corresponding Feynman diagram is shown in Figure 1 in the upper row on the left-hand side. From (A.1) one observes that the probability for emitting a gluon is flat in phase space. In contrast, the real emission contribution to the differential decay rate $h \rightarrow b\bar{b}g$ in the SM is divergent when the radiated gluon becomes unresolved, i.e. soft or collinear to one of the bottom quarks, and therefore such emissions are favoured. As a result, configurations where the total invariant mass $m_{b\bar{b}g} = m_h$ of the $b\bar{b}g$ system is shared equally between the three individual partons occur much more frequently in the former than in the latter case, where the bottom quarks typically carry most of the energy which leads to an invariant mass distribution that is strongly peaked at $m_{b\bar{b}} \simeq m_h$. We add that changing the sign of c_{bH} or c_{bG} will also change the sign of the relative corrections due to the considered SMEFT operators.

Notice that in the case of $c_{bG} \neq 0$ the shape of the $m_{b\bar{b}}$ distribution depends on the jet radius R used to identify b -jets. To illustrate this feature we display in Figure 4 two additional spectra assuming again $c_{bG} = 400$, but taking $R = 0.7$ and $R = 1.0$ instead of the standard choice $R = 0.4$. One observes that the corrections due to Q_{bG} are on average pushed towards lower values of $m_{b\bar{b}}$ when the jet radius R is increased. We further add in this context that at $\mathcal{O}(\alpha_s^3)$ insertions of the operator Q_{bG} lead to a one-loop contribution to the $h \rightarrow b\bar{b}g$ amplitude, tree-level contributions to the $h \rightarrow b\bar{b}q\bar{q}$ and $h \rightarrow b\bar{b}gg$ processes

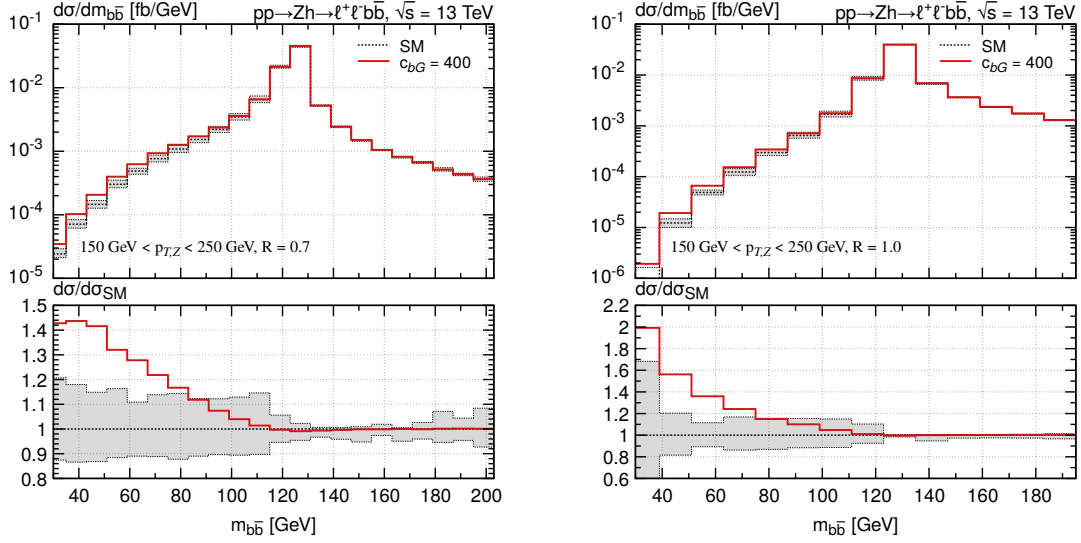


Figure 4: Same as the right panel in Figure 3, but for $R = 0.7$ (left) and $R = 1.0$ (right). See the main text for further details.

and two-loop effects in the $h \rightarrow b\bar{b}$ amplitude (cf. Figure 1). While the two-loop corrections contribute only at $m_{b\bar{b}} = m_h$, the other two types of contributions are again spread over the phase space. Since the $\mathcal{O}(\alpha_s^3)$ non-factorisable corrections due to Q_{bG} are relatively large in the case of the inclusive $h \rightarrow b\bar{b}$ decay width in (4.3), including them in the calculation of the differential cross sections for the full process $pp \rightarrow Zh \rightarrow \ell^+ \ell^- b\bar{b}$ is necessary if one wants to describe kinematic distributions such as $m_{b\bar{b}}$ accurately. We also note that, while the results shown in Figures 3 and 4 have been obtained for $p_{T,Z} \in [150, 250]$ GeV, qualitatively similar modifications of the $m_{b\bar{b}}$ distribution due to Q_{bG} are found when the transverse momentum of the Z boson is restricted to the other two stage 1.2 STXS regions with $p_{T,Z} \in [75, 150]$ GeV and $p_{T,Z} > 250$ GeV. As for the shapes, the observed differences depend on the exact b -jet definition. In fact, they turn out to be more pronounced for a larger radius R .

Another distribution that features interesting shape changes in the presence of a non-zero Wilson coefficient c_{bG} is the invariant mass $m_{b\bar{b}j}$ of the two b -jets and an extra jet. We built this observable from the set of two b -jets and one additional jet whose three-jet invariant mass lies closest to the Higgs boson mass. Figure 5 shows two $m_{b\bar{b}j}$ spectra for $c_{bG} = 400$ with a jet radius of $R = 0.4$ and $R = 0.7$ in the left and the right panel, respectively. Also the modifications in the $m_{b\bar{b}j}$ spectrum due to $c_{bG} \neq 0$ are non-trivial and R -dependent. In fact, the relative SMEFT effects are more pronounced at lower values of $m_{b\bar{b}j}$ and can reach up to around 40%. This feature can be qualitatively understood by remembering that the leading Q_{bg} contributions arise from the process $h \rightarrow b\bar{b}g$, see (A.1), while in the SM the corresponding matrix element is part of the NLO corrections. Relative to the inclusive $h \rightarrow b\bar{b}$ decay width, events with an additional jet will therefore occur more likely in SMEFT scenarios with $c_{bG} \neq 0$ than in the SM. Moreover, since the largest

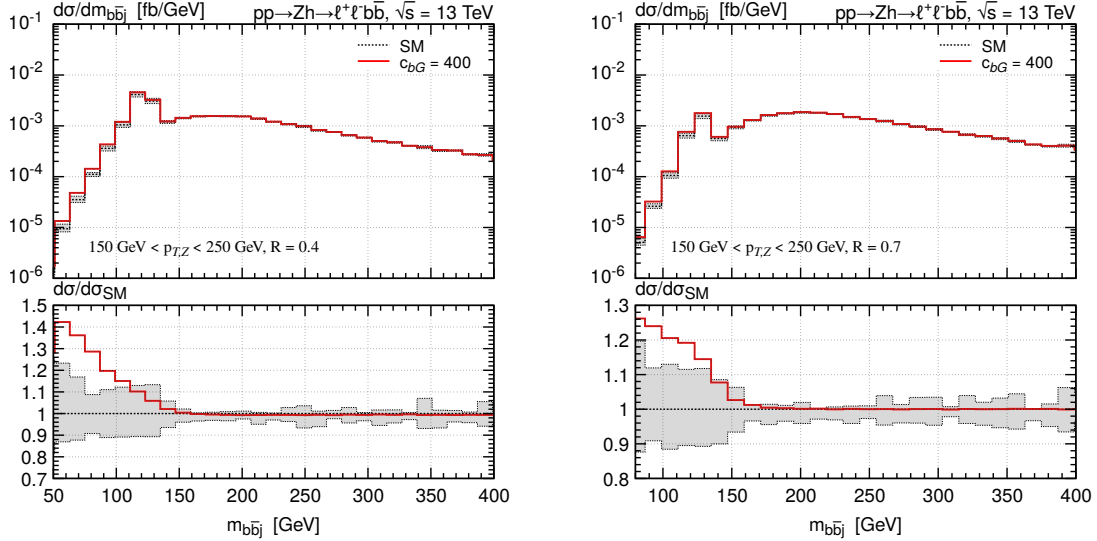


Figure 5: Same as Figure 4, but for $m_{b\bar{b}j}$ using $R = 0.4$ (left panel) and $R = 0.7$ (right panel). See the main text for further details.

corrections in the invariant mass distributions of the two b -jets arise at $m_{b\bar{b}} \simeq 40$ GeV (cf. the right panel in Figure 3 and the two panels in Figure 4) and we impose $p_{T,j} > 25$ GeV, one expects to see an excess of events at $m_{b\bar{b}j} \simeq 60$ GeV. Indeed, this is what is observed in the left panel of Figure 5. It is also clearly visible from the two plots in Figure 5 that increasing the jet radius from $R = 0.4$ to $R = 0.7$ will result in a migration of events to higher $m_{b\bar{b}j}$ values, since a larger jet radius will collect more radiation, leading on average to a larger three-jet invariant mass. We finally mention that in the recent ATLAS analysis [72] of $pp \rightarrow Vh$ production with $h \rightarrow b\bar{b}$ decay the mass $m_{b\bar{b}j}$ of the three-jet system is already used as an input to build the multivariate discriminant in the case of three-jet events (see Table 5 of that publication). We believe that besides $m_{b\bar{b}}$ the variable $m_{b\bar{b}j}$ can play an important role in the context of multivariate discriminants tailored to put constraints on the Wilson coefficient of the operator Q_{bG} .

Let us add that apart from the $m_{b\bar{b}}$ and $m_{b\bar{b}j}$ spectra we have identified additional kinematic distributions that are sensitive to the non-factorisable corrections resulting from the operator Q_{bG} . For instance, also the transverse momentum $p_{T,Z}$ of the Z boson is modified in a non-trivial fashion by $c_{bG} \neq 0$. However, in view of (4.4) the effects in $p_{T,Z}$ cannot exceed the percent level, and therefore this variable taken by itself will have only a rather limited constraining power at the LHC. Similar statements apply to the transverse momentum $p_{T,b\bar{b}}$ of the b -jet pair. Incorporating the latter observables into a multivariate discriminant may however enhance the overall sensitivity to BSM effects associated to $c_{bG} \neq 0$. An analysis of this issue is clearly beyond the scope of this article. Likewise we also do not attempt to derive bounds on the Wilson coefficients c_{bH} and c_{bG} using existing [1, 2, 71, 72] or hypothetical [3, 4] differential LHC data, leaving such an exercise for future research.

5 Conclusions

In this article, we have presented novel predictions for the $pp \rightarrow Zh \rightarrow \ell^+ \ell^- b\bar{b}$ process within the SMEFT. NNLO QCD corrections for both $pp \rightarrow Zh$ production and $h \rightarrow b\bar{b}$ decay have been calculated for a subset of six dimension-six operators appearing in the full SMEFT Lagrangian. These fixed-order predictions have been consistently matched to a PS, allowing for a realistic exclusive description of the process at the level of hadronic events while retaining NNLO QCD accuracy. All SMEFT corrections that are associated to the considered operators and can exceed a percent at the level of the total rate after taking into account the existing experimental bounds on the relevant Wilson coefficients have been implemented into a dedicated MC generator.

Using our NNLO+PS generator we have performed a phenomenological study of the impact of SMEFT contributions on several kinematic distributions in $pp \rightarrow Zh \rightarrow \ell^+ \ell^- b\bar{b}$ production considering simple benchmark scenarios. First, we have employed our calculation to extend the SMEFT computation of the inclusive $h \rightarrow b\bar{b}$ decay width [12] to $\mathcal{O}(\alpha_s^3)$ in the five-flavour scheme. Our result for the N³LO corrections due to the chromomagnetic dipole-type operator Q_{bG} is new. These higher-order QCD effects enhance the numerical impact of Q_{bG} by about 60% compared to the $\mathcal{O}(\alpha_s^2)$ contributions that were known before. In our phenomenological analysis of differential distributions in $pp \rightarrow Zh \rightarrow \ell^+ \ell^- b\bar{b}$ production we have considered explicitly the $m_{b\bar{b}}$ and $m_{b\bar{b}j}$ spectra and illustrated how SMEFT effects can change both the normalisation and the shape of these distributions. While the factorisable corrections associated to the operators $Q_{H\Box}$, Q_{HD} and Q_{bH} act as an overall rescaling factor on all kinematic observables, the non-factorisable contributions that arise from the operator Q_{bG} in (2.1) lead to non-trivial modifications on the shapes of certain distributions. By studying the dependence on the jet radius R that enters the anti- k_t jet clustering algorithm, we have shown that these shape changes depend on the b -jet definition, a feature that to our knowledge has not been discussed in the SMEFT context before. It might be possible to exploit the observed R -dependence of the kinematic distributions such as $m_{b\bar{b}}$ or $m_{b\bar{b}j}$ to enhance the LHC sensitivity to the operator Q_{bG} that is at present only very weakly constrained. Furthermore, combining the invariant masses $m_{b\bar{b}}$ and $m_{b\bar{b}j}$ with other observables such as $p_{T,Z}$ and $p_{T,b\bar{b}}$ in multivariate discriminants that describe the full kinematics of the selected events is likely to enhance the sensitivity of the LHC to BSM realisations with a non-zero Wilson coefficient c_{bG} .⁴ Since we believe that our MC generator should prove useful for everyone interested in comparing LHC data to high-precision SMEFT predictions, we will make the relevant codes to simulate NNLO+PS events for the $pp \rightarrow Zh \rightarrow \ell^+ \ell^- b\bar{b}$ process in the SMEFT publicly available within the POWHEG-BOX framework [76].

Our analysis of SMEFT effects in the $pp \rightarrow Zh \rightarrow \ell^+ \ell^- b\bar{b}$ process includes only a limited subset of dimension-six operators. For instance effective interactions that modify the couplings of the Higgs to EW gauge bosons are not considered in this work. Since it is known [8–10, 15–17] that the latter type of SMEFT contributions can lead to phenomeno-

⁴At future e^+e^- colliders it might be possible to exploit global event-shape variables in the $h \rightarrow b\bar{b}$ decay [75] to put constraints on the Wilson coefficient c_{bG} .

logical relevant effects in Zh production, we plan to apply the discussed NNLO+PS method to non-trivial insertions of purely EW operators as well. Since the leading EW operators contributing to Zh production play only a minor role in the $h \rightarrow b\bar{b}$ decay and vice versa, obtaining NNLO+PS accuracy for a suitable enlarged set of dimension-six operators in the SMEFT seems possible following the methodology developed here.

Acknowledgments

We are grateful to Rhorry Gauld for helpful discussions and useful comments that helped us to improve the manuscript. We also thank Marumi Kado for interesting conversations. The simulations related to this work have used the Max Planck Computing and Data Facility (MPCDF) in Garching. Silvia Zanoli is supported by the International Max Planck Research School (IMPRS) on ‘‘Elementary Particle Physics’’.

A Squared matrix elements

Below we provide the expressions for the squared matrix elements for the non-factorisable SMEFT terms of $\mathcal{O}(y_b^2 C_{bG})$ to the $h \rightarrow b\bar{b}$ decay distributions that are included in our NNLO+PS generator. All matrix elements are computed using conventional dimensional regularisation for both UV and IR singularities in $d = 4 - 2\epsilon$ dimensions with $\overline{\text{MS}}$ subtraction. The actual generation and computation of squared matrix elements relies on the *Mathematica* packages *FeynRules* [77], *FeynArts* [78], *FormCalc* [79, 80], *Package-X* [81] and *LiteRed* [82] as well as *VSM*.

The interference term between the tree-level matrix elements of $h(p_h) \rightarrow b(p_1)\bar{b}(p_2)g(p_3)$ with an insertion of Q_{bG} and the corresponding SM contribution gives rise to a contribution of $\mathcal{O}(y_b^2 \alpha_s^2 C_{bG})$. It takes the following form

$$\mathcal{S}_{b\bar{b}g}^{(0)} = 2\text{Re} \left\langle \mathcal{M}_{y_b, b\bar{b}g}^{(0)} \left| \mathcal{M}_{C_{bG}, b\bar{b}g}^{(0)} \right. \right\rangle = 8\alpha_s^2 C_F C_A m_h^2 y_b^2 \frac{\text{Re}(C_{bG})}{\Lambda^2}. \quad (\text{A.1})$$

Here $\mathcal{M}_{y_b, b\bar{b}g}^{(0)}$ and $\mathcal{M}_{C_{bG}, b\bar{b}g}^{(0)}$ denote the SM and SMEFT tree-level $h \rightarrow b\bar{b}g$ matrix element, respectively, and $C_F = 4/3$ and $C_A = 3$ are the relevant colour factors.

At $\mathcal{O}(y_b^2 \alpha_s^3 C_{bG})$ the interference term between the Q_{bG} and the SM contribution to $h(p_h) \rightarrow b(p_1)\bar{b}(p_2)g(p_3)$ can be written as follows

$$\mathcal{S}_{b\bar{b}g}^{(1)} = 2\text{Re} \left\langle \mathcal{M}_{y_b, b\bar{b}g}^{(1)} \left| \mathcal{M}_{C_{bG}, b\bar{b}g}^{(0)} \right. \right\rangle + 2\text{Re} \left\langle \mathcal{M}_{y_b, b\bar{b}g}^{(0)} \left| \mathcal{M}_{C_{bG}, b\bar{b}g}^{(1)} \right. \right\rangle, \quad (\text{A.2})$$

where $\mathcal{M}_{y_b, b\bar{b}g}^{(1)}$ and $\mathcal{M}_{C_{bG}, b\bar{b}g}^{(1)}$ denote the SM and SMEFT one-loop $h \rightarrow b\bar{b}g$ matrix element. To write our result for $\mathcal{S}_{b\bar{b}g}^{(1)}$ in a compact form we will use

$$y_{ij} = \frac{2p_i \cdot p_j}{m_h^2}, \quad (\text{A.3})$$

i.e. twice the dot-product of two external four-momenta p_i and p_j divided by the Higgs boson mass squared. For the sum of terms in (A.2) we obtain

$$\begin{aligned}
\mathcal{S}_{b\bar{b}g}^{(1)} = \frac{\alpha_s}{2\pi} N_\epsilon \mathcal{S}_{b\bar{b}g}^{(0)} & \left\{ -\frac{2C_F + C_A}{\epsilon^2} - \frac{1}{\epsilon} \left[(C_A - 2C_F) L_{12} - C_A (L_{13} + L_{23}) + \gamma_g + 2\gamma_q \right] \right. \\
& + (C_A - 2C_F) \left[\frac{1}{2} R(y_{12}, y_{13}) + \frac{1}{2} R(y_{12}, y_{23}) + \frac{L_{12}^2}{2} - L_{12} \right] \\
& - C_A \left[\frac{1}{2} R(y_{13}, y_{23}) + \frac{L_{13}^2}{2} + \frac{L_{23}^2}{2} \right] - C_F (1 - L_{13} - L_{23}) \\
& \left. + 3(2C_F + C_A) \zeta_2 + \frac{1}{2} (C_A - C_F) (y_{13} + y_{23}) + \gamma_{bG} + (\gamma_g + 2\gamma_q + \gamma_{bG}) L \right\}.
\end{aligned} \tag{A.4}$$

Here we have defined

$$N_\epsilon = \frac{e^{\epsilon\gamma_E}}{\Gamma(1-\epsilon)} \left(\frac{\mu^2}{m_h^2} \right)^\epsilon = 1 + L\epsilon + [L^2 - \zeta_2] \frac{\epsilon^2}{2}, \tag{A.5}$$

where $\Gamma(z)$ is the gamma function, $\gamma_E \simeq 0.577$ is the Euler-Mascheroni constant, $\zeta_2 = \pi^2/6$ is the Riemann Zeta function of two and

$$L_{ij} = \ln y_{ij}, \quad L = \ln \frac{\mu^2}{m_h^2}. \tag{A.6}$$

We have furthermore introduced

$$R(x, y) = \text{Li}_2(1-x) + \text{Li}_2(1-y) + \ln x \ln y - \zeta_2, \tag{A.7}$$

with $\text{Li}_2(z)$ the dilogarithm. The anomalous dimensions γ_g and γ_q appearing in (A.4) can for example be found in the classic work [83] on the IR structure of QCD scattering amplitudes, while calculations of the anomalous dimension of the operator Q_{bG} have been performed in [84, 85]. The needed anomalous dimensions read

$$\gamma_g = \frac{11C_A}{6} - \frac{N_f}{3}, \quad \gamma_q = \frac{3C_F}{2}, \quad \gamma_{bG} = 2C_A - 8C_F, \tag{A.8}$$

where N_f denotes the number of active quark flavours. We add that as a cross-check of our SMEFT calculation, we have also computed the interference between the tree-level and one-loop $h \rightarrow b\bar{b}g$ matrix elements in the SM. Our SM calculation reproduces the expression given in (A.6) of the publication [27].⁵

We also need the $\mathcal{O}(y_b^2 \alpha_s^3 C_{bG})$ interferences for all relevant Higgs to four parton scattering processes. To write these squared tree-level amplitudes in a compact form we introduce

$$y_{ijk} = y_{ij} + y_{ik} + y_{jk}. \tag{A.9}$$

⁵The terms $\ln y_{ij}^2$ in (A.6) of [27] are obvious misprints that should in fact read $\ln^2 y_{ij}$.

For $h(p_h) \rightarrow b(p_1)\bar{b}(p_2)q(p_3)\bar{q}(p_4)$, we obtain

$$\mathcal{S}_{b\bar{b}q\bar{q}}^{(0)} = 2\text{Re} \left\langle \mathcal{M}_{y_b, b\bar{b}q\bar{q}}^{(0)} \left| \mathcal{M}_{C_{bG}, b\bar{b}q\bar{q}}^{(0)} \right. \right\rangle = 2\pi\alpha_s \mathcal{S}_{b\bar{b}g}^{(0)} \frac{1}{m_h^2} g_{b\bar{b}q\bar{q}}(p_1, p_2, p_3, p_4), \quad (\text{A.10})$$

where

$$g_{b\bar{b}q\bar{q}}(p_1, p_2, p_3, p_4) = -\frac{y_{13}}{y_{234}} + \frac{y_{13}}{y_{34}y_{134}} - \frac{2y_{24}y_{13}}{y_{134}y_{234}} - \frac{(y_{14}y_{23} + 3y_{13}y_{24})y_{13}}{y_{34}y_{134}y_{234}} \\ - \frac{y_{24}(y_{13}y_{24} - y_{14}y_{23})y_{13}}{y_{34}^2y_{134}y_{234}} + (1 \leftrightarrow 2) + (3 \leftrightarrow 4) + (1 \leftrightarrow 2, 3 \leftrightarrow 4). \quad (\text{A.11})$$

In the case of $h(p_h) \rightarrow b(p_1)\bar{b}(p_2)b(p_3)\bar{b}(p_4)$, we find

$$\mathcal{S}_{b\bar{b}b\bar{b}}^{(0)} = 2\text{Re} \left\langle \mathcal{M}_{y_b, b\bar{b}b\bar{b}}^{(0)} \left| \mathcal{M}_{C_{bG}, b\bar{b}b\bar{b}}^{(0)} \right. \right\rangle \\ = 2\pi\alpha_s \mathcal{S}_{b\bar{b}g}^{(0)} \frac{1}{m_h^2} \left[(C_A - 2C_F) f_{b\bar{b}b\bar{b}}(p_1, p_2, p_3, p_4) + g_{b\bar{b}b\bar{b}}(p_1, p_2, p_3, p_4) \right], \quad (\text{A.12})$$

where

$$f_{b\bar{b}b\bar{b}}(p_1, p_2, p_3, p_4) = \frac{y_{12}^5}{y_{14}y_{123}y_{124}y_{134}y_{234}} + \frac{y_{12}^5}{y_{23}y_{123}y_{124}y_{134}y_{234}} + \frac{(4y_{13} + y_{23} + 2y_{24} - 1)y_{12}^4}{y_{14}y_{123}y_{124}y_{134}y_{234}} \\ + \frac{(y_{13} + y_{14} + 4y_{24} - 1)y_{12}^4}{y_{23}y_{123}y_{124}y_{134}y_{234}} + \frac{y_{13}(y_{23} + 3y_{24} - 4)y_{12}^3}{y_{14}y_{123}y_{124}y_{134}y_{234}} - \frac{(2y_{13} + y_{14} + y_{23} + y_{24} + 2y_{34})y_{12}^3}{y_{123}y_{124}y_{134}y_{234}} \\ + \frac{(y_{24}(2y_{13} + y_{14} + 6y_{24} - 4) - y_{14}y_{34})y_{12}^3}{y_{23}y_{123}y_{124}y_{134}y_{234}} + \frac{(y_{24}(y_{23} + y_{24} - 1) - y_{23}y_{34})y_{12}^3}{y_{14}y_{123}y_{124}y_{134}y_{234}} \\ + \frac{6y_{13}^2y_{12}^3}{y_{14}y_{123}y_{124}y_{134}y_{234}} + \frac{y_{13}y_{24}^2y_{12}^3}{y_{23}y_{34}y_{123}y_{124}y_{134}y_{234}} + \frac{y_{13}^2y_{24}y_{12}^3}{y_{14}y_{34}y_{123}y_{124}y_{134}y_{234}} \\ - \frac{(y_{13}y_{23} - 2y_{14}y_{23} + 2y_{13}y_{24} + y_{14}y_{24})y_{12}^3}{y_{34}y_{123}y_{124}y_{134}y_{234}} - \frac{y_{13}^2y_{12}^2}{y_{123}y_{124}y_{134}y_{234}} - \frac{y_{13}^2y_{24}y_{12}^2}{y_{23}y_{123}y_{124}y_{134}y_{234}} \\ + \frac{y_{13}^2(3y_{24} - 4)y_{12}^2}{y_{14}y_{123}y_{124}y_{134}y_{234}} - \frac{y_{24}^2y_{34}y_{12}^2}{y_{14}y_{123}y_{124}y_{134}y_{234}} + \frac{(4y_{24}^3 - 4y_{24}^2 - y_{34}(5y_{14} + y_{34})y_{24} + 2y_{14}y_{34}^2)y_{12}^2}{y_{23}y_{123}y_{124}y_{134}y_{234}} \\ + \frac{y_{13}(3y_{24}^2 - 4y_{34}y_{24} - y_{34} + y_{14}(y_{34} - 5y_{24}))y_{12}^2}{y_{23}y_{123}y_{124}y_{134}y_{234}} - \frac{y_{13}(3y_{14} + 9y_{23} + 4(3y_{24} + y_{34}))y_{12}^2}{y_{123}y_{124}y_{134}y_{234}} \\ - \frac{y_{13}(5y_{23}(y_{24} + y_{34}) + y_{24}(y_{24} + 5y_{34}))y_{12}^2}{y_{14}y_{123}y_{124}y_{134}y_{234}} + \frac{(y_{14}^2 - 9y_{24}y_{14} + y_{23}^2 - y_{24}(3y_{23} + y_{24} + 5y_{34}))y_{12}^2}{y_{123}y_{124}y_{134}y_{234}} \\ + \frac{3y_{13}^3y_{12}^2}{y_{14}y_{123}y_{124}y_{134}y_{234}} - \frac{2y_{13}^2y_{23}y_{12}^2}{y_{34}y_{123}y_{124}y_{134}y_{234}} + \frac{y_{13}y_{24}^2(3(y_{13} + y_{14}) + 2y_{24})y_{12}^2}{y_{23}y_{34}y_{123}y_{124}y_{134}y_{234}} \\ - \frac{y_{13}(3y_{24}^2 + 5(y_{14} + y_{23})y_{24})y_{12}^2}{y_{34}y_{123}y_{124}y_{134}y_{234}} + \frac{y_{14}(-2y_{24}^2 - 3y_{14}y_{24} + 2y_{23}(y_{14} + y_{23}))y_{12}^2}{y_{34}y_{123}y_{124}y_{134}y_{234}} \\ + \frac{y_{13}^2y_{24}(2y_{13} + 3(y_{23} + y_{24}))y_{12}^2}{y_{14}y_{34}y_{123}y_{124}y_{134}y_{234}} - \frac{y_{13}^3y_{12}}{y_{123}y_{124}y_{134}y_{234}} + \frac{(y_{24} - 1)y_{24}^3y_{12}}{y_{23}y_{123}y_{124}y_{134}y_{234}}$$

$$\begin{aligned}
& + \frac{y_{13}y_{24}(y_{13}+y_{24})(2y_{13}+y_{24})y_{12}}{y_{14}y_{123}y_{124}y_{134}y_{234}} - \frac{y_{13}(y_{24}^2+4(y_{14}+y_{23})y_{24}+6y_{14}y_{23})y_{12}}{y_{123}y_{124}y_{134}y_{234}} \\
& + \frac{3y_{13}y_{24}^2(y_{24}-y_{34})y_{12}}{y_{23}y_{123}y_{124}y_{134}y_{234}} + \frac{3y_{13}^2y_{24}(y_{24}-y_{34})y_{12}}{y_{23}y_{123}y_{124}y_{134}y_{234}} + \frac{y_{13}^3(y_{24}-y_{34})y_{12}}{y_{23}y_{123}y_{124}y_{134}y_{234}} \\
& - \frac{y_{13}^2(3y_{14}+4y_{23}+y_{24}+4y_{34})y_{12}}{y_{123}y_{124}y_{134}y_{234}} - \frac{y_{24}(6y_{14}y_{23}+3y_{24}y_{23}+4y_{14}y_{24}+4y_{24}y_{34})y_{12}}{y_{123}y_{124}y_{134}y_{234}} \\
& - \frac{3y_{14}y_{23}y_{24}^2y_{12}}{y_{34}y_{123}y_{124}y_{134}y_{234}} + \frac{2y_{13}^3y_{24}^2y_{12}}{y_{23}y_{34}y_{123}y_{124}y_{134}y_{234}} - \frac{y_{13}^3(y_{23}-3y_{24})y_{12}}{y_{34}y_{123}y_{124}y_{134}y_{234}} \\
& + \frac{y_{13}^4y_{24}y_{12}}{y_{14}y_{34}y_{123}y_{124}y_{134}y_{234}} + \frac{y_{13}y_{24}^3(2y_{14}+y_{24})y_{12}}{y_{23}y_{34}y_{123}y_{124}y_{134}y_{234}} + \frac{y_{13}^2y_{24}^2(3y_{23}+2y_{24})y_{12}}{y_{14}y_{34}y_{123}y_{124}y_{134}y_{234}} \\
& + \frac{y_{13}^2y_{24}^2(3y_{14}+5y_{24})y_{12}}{y_{23}y_{34}y_{123}y_{124}y_{134}y_{234}} + \frac{y_{13}^3y_{24}(2y_{23}+5y_{24})y_{12}}{y_{14}y_{34}y_{123}y_{124}y_{134}y_{234}} + \frac{y_{13}^2(6y_{24}^2-2y_{14}y_{24}-3y_{14}y_{23})y_{12}}{y_{34}y_{123}y_{124}y_{134}y_{234}} \\
& + \frac{y_{13}y_{24}(y_{24}(3y_{24}-2y_{23})-8y_{14}y_{23})y_{12}}{y_{34}y_{123}y_{124}y_{134}y_{234}} + \frac{2y_{13}y_{24}(y_{13}^2+y_{24}^2)}{y_{123}y_{124}y_{134}y_{234}} + \frac{y_{13}^2y_{24}^3(y_{13}+y_{24})}{y_{23}y_{34}y_{123}y_{124}y_{134}y_{234}} \\
& + \frac{y_{13}^3y_{24}^2(y_{13}+y_{24})}{y_{14}y_{34}y_{123}y_{124}y_{134}y_{234}} + \frac{y_{13}y_{24}(y_{13}+y_{24})(y_{13}^2+3y_{24}y_{13}+y_{24}^2)}{y_{34}y_{123}y_{124}y_{134}y_{234}} \\
& + (1 \leftrightarrow 3) + (2 \leftrightarrow 4) + (1 \leftrightarrow 3, 2 \leftrightarrow 4). \tag{A.13}
\end{aligned}$$

Furthermore,

$$g_{\bar{b}\bar{b}\bar{b}\bar{b}}(p_1, p_2, p_3, p_4) = g_{\bar{b}\bar{b}\bar{q}\bar{q}}(p_1, p_2, p_3, p_4) + (1 \leftrightarrow 3) + (2 \leftrightarrow 4) + (1 \leftrightarrow 3, 2 \leftrightarrow 4), \tag{A.14}$$

with $g_{\bar{b}\bar{b}\bar{q}\bar{q}}(p_1, p_2, p_3, p_4)$ already defined in (A.11).

For the process $h(p_h) \rightarrow b(p_1)\bar{b}(p_2)g(p_3)g(p_4)$, we finally get

$$\begin{aligned}
\mathcal{S}_{\bar{b}\bar{b}g\bar{g}}^{(0)} &= 2\text{Re} \left\langle \mathcal{M}_{y_b, \bar{b}\bar{b}g\bar{g}}^{(0)} \left| \mathcal{M}_{C_{bG}, \bar{b}\bar{b}g\bar{g}}^{(0)} \right. \right\rangle \\
&= 2\pi\alpha_s \mathcal{S}_{\bar{b}\bar{b}g}^{(0)} \frac{1}{m_h^2} \left[C_A f_{\bar{b}\bar{b}g\bar{g}}(p_1, p_2, p_3, p_4) + C_F g_{\bar{b}\bar{b}g\bar{g}}(p_1, p_2, p_3, p_4) \right]. \tag{A.15}
\end{aligned}$$

Here

$$\begin{aligned}
f_{\bar{b}\bar{b}g\bar{g}}(p_1, p_2, p_3, p_4) &= \frac{4y_{24}^2}{y_{23}y_{34}y_{234}} + \frac{y_{13}^2y_{24}^2}{2y_{14}y_{23}y_{34}y_{134}y_{234}} + \frac{(10y_{13}+9y_{34})y_{24}}{y_{14}y_{134}y_{234}} \\
& + \frac{(4y_{24}+19y_{34}-4)y_{24}}{y_{23}y_{134}y_{234}} + \frac{(4y_{14}(y_{23}+2)+y_{13}(12y_{24}+7))y_{24}}{2y_{34}y_{134}y_{234}} + \frac{2y_{13}(y_{13}y_{24}-y_{14}y_{23})y_{24}}{y_{34}^2y_{134}y_{234}} \\
& - \frac{2y_{34}^2}{y_{13}y_{14}y_{134}} + \frac{y_{34}^2(y_{23}+y_{24}+y_{34}-1)}{y_{13}y_{14}y_{23}y_{134}} + \frac{y_{34}^2(y_{23}+3y_{24}+2y_{34})}{y_{13}y_{14}y_{134}y_{234}} \\
& + \frac{18y_{34}+2y_{24}(4y_{13}+2y_{23}+2y_{24}+2y_{34}+19)-3}{2y_{134}y_{234}} + \frac{12y_{14}y_{24}+5y_{34}(2y_{24}+3y_{34}-1)}{y_{13}y_{134}y_{234}} \\
& + \frac{2y_{14}y_{24}(2y_{24}+3y_{34}-1)+y_{34}(3y_{34}^2+(9y_{24}-2)y_{34}+4(y_{24}-1)y_{24})}{y_{13}y_{23}y_{134}y_{234}}
\end{aligned}$$

$$\begin{aligned}
& + \frac{(y_{13}y_{24}(6y_{24} + 8y_{34} - 1) + y_{34}(6y_{24}^2 + 2(7y_{34} - 2)y_{24} + y_{34}(5y_{34} - 3)))}{2y_{14}y_{23}y_{134}y_{234}} \\
& + (1 \leftrightarrow 2) + (3 \leftrightarrow 4) + (1 \leftrightarrow 2, 3 \leftrightarrow 4), \tag{A.16}
\end{aligned}$$

while

$$\begin{aligned}
g_{b\bar{b}g\bar{g}}(p_1, p_2, p_3, p_4) = & -\frac{2(y_{23} + y_{24} + y_{34} - 1)y_{34}^2}{y_{13}y_{14}y_{23}y_{134}} + \frac{4y_{34}^2}{y_{13}y_{14}y_{134}} - \frac{2(y_{23} + 3y_{24} + 2y_{34})y_{34}^2}{y_{13}y_{14}y_{134}y_{234}} \\
& + \frac{2y_{24}(-4y_{24} + (y_{34} - 14)y_{34} + 4)}{y_{23}y_{134}y_{234}} + \frac{2y_{24}(y_{34}(y_{24} + 2y_{34} - 7) + y_{13}(y_{24} + 2y_{34} - 5))}{y_{14}y_{134}y_{234}} \\
& + \frac{2(3y_{24}^2 + (4y_{13} + 4y_{14} + 3y_{23} + 13y_{34} - 14)y_{24} + y_{34}(3y_{34} - 8) + 2)}{y_{134}y_{234}} \\
& - \frac{2(2y_{14}y_{24}(2y_{24} + 3y_{34} - 1) + y_{34}(3y_{34}^2 + (9y_{24} - 2)y_{34} + 4(y_{24} - 1)y_{24}))}{y_{13}y_{23}y_{134}y_{234}} \\
& + \frac{2(y_{14}y_{24}(y_{23} + y_{34} - 8) + y_{34}(y_{24}^2 + (2y_{23} + 2y_{34} - 9)y_{24} + (y_{34} - 13)y_{34} + 5))}{y_{13}y_{134}y_{234}} \\
& - \frac{2(y_{13}y_{24}(y_{24} + 2y_{34}) + y_{34}(2y_{24}^2 + (5y_{34} - 1)y_{24} + y_{34}(2y_{34} - 1)))}{y_{14}y_{23}y_{134}y_{234}} \\
& + (1 \leftrightarrow 2) + (3 \leftrightarrow 4) + (1 \leftrightarrow 2, 3 \leftrightarrow 4). \tag{A.17}
\end{aligned}$$

As a cross-check of our SMEFT computation we have also calculated the squared matrix elements for the tree-level processes $h \rightarrow b\bar{b}q\bar{q}$, $h \rightarrow b\bar{b}b\bar{b}$ and $h \rightarrow b\bar{b}g\bar{g}$ within the SM. Our findings agree with (A.8), (A.9), (A.11), (A.13), (A.14) and (A.16) of [27].

In the case of the $h(p_h) \rightarrow b(p_1)\bar{b}(p_2)$ transition, the first non-zero contribution to the interference with an insertion of Q_{bG} and the corresponding SM contribution arises at $\mathcal{O}(y_b^2 \alpha_s^3 C_{bG})$. We find

$$\mathcal{S}_{b\bar{b}}^{(2)} = 2\text{Re} \left\langle \mathcal{M}_{y_b, b\bar{b}}^{(0)} \left| \mathcal{M}_{C_{bG}, b\bar{b}}^{(2)} \right. \right\rangle = -\frac{\alpha_s}{256\pi^3} N_\epsilon^2 \mathcal{S}_{b\bar{b}g}^{(0)} m_h^2 \gamma_{bG} (7 + 2L), \tag{A.18}$$

where $\mathcal{M}_{C_{bG}, b\bar{b}}^{(2)}$ denotes the relevant two-loop $h \rightarrow b\bar{b}$ matrix element in the SMEFT and the expressions for $\mathcal{S}_{b\bar{b}g}^{(0)}$, N_ϵ and γ_{bG} have been given in (A.1), (A.5) and (A.8), respectively.

B Numerical impact of C_{HG} and C_{3G}

In this appendix we assess the numerical impact of the dimension-six operators Q_{HG} and Q_{3G} on the $h \rightarrow b\bar{b}$ decay and the $pp \rightarrow Zh$ production process. Since we show below that these operators contribute to less than a percent at the level of total rates once existing experimental limits on the relevant Wilson coefficients are taken into account, the effects of Q_{HG} and Q_{3G} have been neglected in the phenomenological analysis carried out in the main part of this work.

The leading correction to the inclusive $h \rightarrow b\bar{b}$ decay rate proportional to the Wilson coefficient C_{HG} has been calculated for massive bottom quarks in [12]. Example diagrams

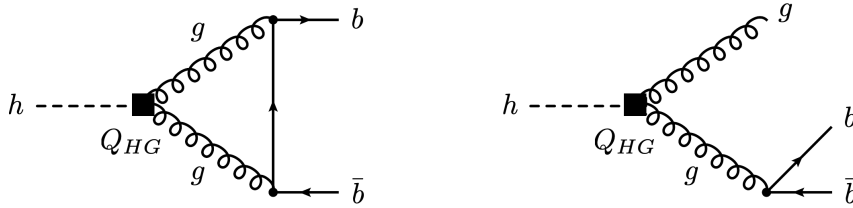


Figure 6: Examples of SMEFT contributions to the inclusive decay rate of $h \rightarrow b\bar{b}$ with an insertion of Q_{HG} (black square). The left (right) diagram represents a one-loop (tree-level) contribution to the $h \rightarrow b\bar{b}$ ($h \rightarrow b\bar{b}g$) transition.

are shown in Figure 6. Employing the operator basis (2.1) and working to leading power in m_b one finds at NNLO in QCD the simple expression

$$\Gamma(h \rightarrow b\bar{b})_{\text{SMEFT}}^{\text{NNLO},HG} = \left(\frac{\alpha_s}{\pi}\right)^2 \left[\frac{19}{3} - 2\zeta_2 + \frac{1}{3} \ln^2\left(\frac{\bar{m}_b^2}{m_h^2}\right) \right] c_{HG} \Gamma(h \rightarrow b\bar{b})_{\text{SM}}^{\text{LO}}, \quad (\text{B.1})$$

where the definition of the Wilson coefficient c_{HG} can be found in (3.14). A recent global fit [62] to the SMEFT including 34 dimension-six operators reports the following marginalised 95% CL bound

$$c_{HG} \in [-0.09, 0.06], \quad (\text{B.2})$$

on the relevant Wilson coefficient (cf. Table 6 of the latter work). Using this limit together with the input parameters given at the beginning of Section 4 it follows from (B.1) and (B.2) that at 95% CL the Q_{HG} contribution to the inclusive $h \rightarrow b\bar{b}$ decay rate lies within

$$\frac{\Gamma(h \rightarrow b\bar{b})_{\text{SMEFT}}^{\text{NNLO},HG}}{\Gamma(h \rightarrow b\bar{b})_{\text{SM}}^{\text{LO}}} \in [-2.7, 1.7] \cdot 10^{-3}. \quad (\text{B.3})$$

This result indicates that SMEFT effects arising from Q_{HG} are phenomenologically irrelevant in the case of the fully differential $h \rightarrow b\bar{b}$ decay rate. This justifies that we have neglected such corrections in the main part of this article.

Operator insertions of Q_{3G} induce tree-level contributions to $h \rightarrow b\bar{b}gg$ and one-loop corrections to $h \rightarrow b\bar{b}g$. After interfering these channels with the corresponding SM amplitudes and integrating over the four- and three-particle phase space, respectively, the combination of these two types of contributions leads to a N³LO correction to the inclusive $h \rightarrow b\bar{b}$ decay rate. We write the sum of these real and virtual corrections as

$$\Gamma(h \rightarrow b\bar{b})_{\text{SMEFT}}^{\text{N}^3\text{LO},3G} = N_{3G}^{\text{dec}} \left(\frac{\alpha_s}{\pi}\right)^3 \frac{m_h^2}{v^2} c_{3G} \Gamma(h \rightarrow b\bar{b})_{\text{SM}}^{\text{LO}}, \quad (\text{B.4})$$

where we have defined

$$c_{3G} = \frac{v^2}{\Lambda^2} C_{3G}. \quad (\text{B.5})$$

The marginalised 95% CL limit on the relevant Wilson coefficient reads [62]⁶

$$c_{3G} \in [-12.5, -4.1]. \quad (\text{B.6})$$

⁶The large negative values of c_{3G} found in the work [62] can be traced back to the discrepancy between the measured $t\bar{t}$ differential cross section [86] and the state-of-the-art SM prediction [87] at large values of the top-antitop invariant mass $m_{t\bar{t}}$. Analyses of multijet data [88–90] suggest bounds of $|c_{3G}| \lesssim 0.2$.

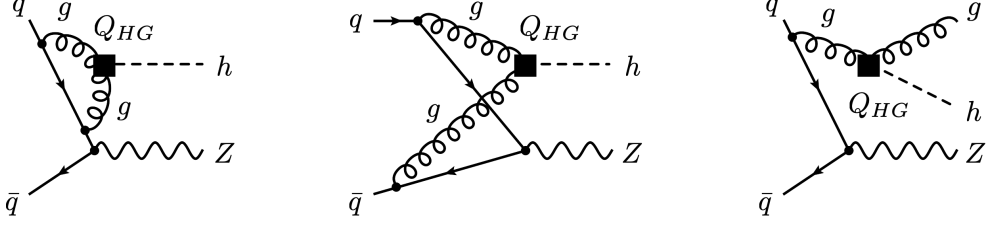


Figure 7: Examples of SMEFT contributions to Zh production involving an insertion of Q_{HG} (black square). The left and middle (right) diagram represent(s) a one-loop (tree-level) contribution to the $q\bar{q} \rightarrow Zh$ ($q\bar{q} \rightarrow Zhg$) process.

Plugging (B.6) into (B.4) then leads to

$$\frac{\Gamma(h \rightarrow b\bar{b})_{\text{SMEFT}}^{\text{N}^3\text{LO},3G}}{\Gamma(h \rightarrow b\bar{b})_{\text{SM}}^{\text{LO}}} \in [-0.15, -0.05] \cdot 10^{-3} N_{3G}^{\text{dec}}. \quad (\text{B.7})$$

By performing an explicit calculation of the tree-level contributions to $h \rightarrow b\bar{b}gg$ and the one-loop corrections to $h \rightarrow b\bar{b}g$ associated to insertions of Q_{3G} , we find for the unknown constant N_{3G}^{dec} introduced in (B.4) the numerical value $N_{3G}^{\text{dec}} = 2.23$. This implies that the relative corrections associated to the operator Q_{3G} do not even reach the level of a permille. Neglecting these corrections as done in our SMEFT analysis of the fully differential $h \rightarrow b\bar{b}$ decay rate is therefore fully justified from a phenomenological point of view.

The leading corrections to Zh production associated to the operator Q_{HG} result from the Feynman graphs displayed in Figure 7. These types of diagrams have been calculated in the context of the SM in [50] working in the limit of infinite top-quark mass. Using the results of the latter work one can write the $\mathcal{O}(\alpha_s^2 C_{HG})$ corrections to the inclusive Zh production cross section in the following way

$$\sigma(pp \rightarrow Zh)_{\text{SMEFT}}^{\text{NNLO},HG} = 3 \left(\frac{\alpha_s}{\pi} \right)^2 \delta c_{HG} \sigma(pp \rightarrow Zh)_{\text{SM}}^{\text{LO}}, \quad (\text{B.8})$$

where $\sigma(pp \rightarrow Zh)_{\text{SM}}^{\text{LO}}$ is the LO cross section and δ encodes the sum of the QCD corrections denoted by V_{I} and R_{I} in [50] with a factor of $(\alpha_s/\pi)^2$ stripped off. We add that we have calculated the relevant radiative corrections that give rise to V_{I} and R_{I} finding agreement with the latter publication (see also [91, 92]). Notice that an expression analogous to (B.8) also holds for the differential cross section. From Figure 6 of the paper [50] one finds that at the LHC one has $\delta = 10.7$ for the measured mass of the Higgs boson. This corresponds to a 1.4% correction in the SM. Using the limit (B.2) in (B.8) we obtain

$$\frac{\sigma(pp \rightarrow Zh)_{\text{SMEFT}}^{\text{NNLO},HG}}{\sigma(pp \rightarrow Zh)_{\text{SM}}^{\text{LO}}} \in [-3.9, 2.4] \cdot 10^{-3}, \quad (\text{B.9})$$

at 95% CL. This numerical result shows that it is an excellent approximation to neglect contributions due to Q_{HG} in the calculation of Zh production observables.

Insertions of the operator Q_{3G} induce tree-level contributions to $q\bar{q} \rightarrow Zhgg$ and one-loop corrections to $q\bar{q} \rightarrow Zhg$. Interfering the SMEFT with the corresponding SM amplitudes and integrating over the relevant phase spaces, one obtains a N^3LO correction to

the inclusive Zh production cross section. Using naive dimensional analysis, we write this correction as follows

$$\sigma(pp \rightarrow Zh)_{\text{SMEFT}}^{\text{N}^3\text{LO},3G} = N_{3G}^{\text{prod}} \left(\frac{\alpha_s}{\pi}\right)^3 c_{3G} \sigma(pp \rightarrow Zh)_{\text{SM}}^{\text{LO}}, \quad (\text{B.10})$$

where N_{3G}^{prod} is an undetermined numerical factor which is naively of $\mathcal{O}(1)$. From (B.6) and (B.10) it follows that

$$\frac{\sigma(pp \rightarrow Zh)_{\text{SMEFT}}^{\text{N}^3\text{LO},3G}}{\sigma(pp \rightarrow Zh)_{\text{SM}}^{\text{LO}}} \in [-0.58, -0.19] \cdot 10^{-3} N_{3G}^{\text{prod}}. \quad (\text{B.11})$$

For $N_{3G}^{\text{prod}} = \mathcal{O}(10)$ this 95% CL bound implies a relative correction of a few permille to the inclusive $pp \rightarrow Zh$ cross section. In practice, the N^3LO corrections (B.10) can therefore be neglected.

References

- [1] ATLAS collaboration, *Observation of $H \rightarrow b\bar{b}$ decays and VH production with the ATLAS detector*, *Phys. Lett. B* **786** (2018) 59 [1808.08238].
- [2] CMS collaboration, *Observation of Higgs boson decay to bottom quarks*, *Phys. Rev. Lett.* **121** (2018) 121801 [1808.08242].
- [3] ATLAS collaboration, *Projections for measurements of Higgs boson cross sections, branching ratios, coupling parameters and mass with the ATLAS detector at the HL-LHC*, *ATL-PHYS-PUB-2018-054*.
- [4] CMS collaboration, *Sensitivity projections for Higgs boson properties measurements at the HL-LHC*, *CMS-PAS-FTR-18-011*.
- [5] W. Buchmüller and D. Wyler, *Effective Lagrangian Analysis of New Interactions and Flavor Conservation*, *Nucl. Phys.* **B268** (1986) 621.
- [6] B. Grzadkowski, M. Iskrzynski, M. Misiak and J. Rosiek, *Dimension-Six Terms in the Standard Model Lagrangian*, *JHEP* **10** (2010) 085 [1008.4884].
- [7] I. Brivio and M. Trott, *The Standard Model as an Effective Field Theory*, *Phys. Rept.* **793** (2019) 1 [1706.08945].
- [8] K. Mimasu, V. Sanz and C. Williams, *Higher Order QCD predictions for Associated Higgs production with anomalous couplings to gauge bosons*, *JHEP* **08** (2016) 039 [1512.02572].
- [9] C. Degrande, B. Fuks, K. Mawatari, K. Mimasu and V. Sanz, *Electroweak Higgs boson production in the standard model effective field theory beyond leading order in QCD*, *Eur. Phys. J. C* **77** (2017) 262 [1609.04833].
- [10] S. Alioli, W. Dekens, M. Girard and E. Mereghetti, *NLO QCD corrections to SM-EFT dilepton and electroweak Higgs boson production, matched to parton shower in POWHEG*, *JHEP* **08** (2018) 205 [1804.07407].
- [11] R. Gauld, B.D. Pecjak and D.J. Scott, *One-loop corrections to $h \rightarrow b\bar{b}$ and $h \rightarrow \tau\bar{\tau}$ decays in the Standard Model Dimension-6 EFT: four-fermion operators and the large- m_t limit*, *JHEP* **05** (2016) 080 [1512.02508].

- [12] R. Gauld, B.D. Pecjak and D.J. Scott, *QCD radiative corrections for $h \rightarrow b\bar{b}$ in the Standard Model Dimension-6 EFT*, *Phys. Rev. D* **94** (2016) 074045 [[1607.06354](#)].
- [13] J.M. Cullen, B.D. Pecjak and D.J. Scott, *NLO corrections to $h \rightarrow b\bar{b}$ decay in SMEFT*, *JHEP* **08** (2019) 173 [[1904.06358](#)].
- [14] J.M. Cullen and B.D. Pecjak, *Higgs decay to fermion pairs at NLO in SMEFT*, *JHEP* **11** (2020) 079 [[2007.15238](#)].
- [15] W. Bizoń, F. Caola, K. Melnikov and R. Röntsch, *Anomalous couplings in associated VH production with Higgs boson decay to massive b quarks at NNLO in QCD*, *Phys. Rev. D* **105** (2022) 014023 [[2106.06328](#)].
- [16] F. Maltoni, K. Mawatari and M. Zaro, *Higgs characterisation via vector-boson fusion and associated production: NLO and parton-shower effects*, *Eur. Phys. J. C* **74** (2014) 2710 [[1311.1829](#)].
- [17] A. Greljo, G. Isidori, J.M. Lindert, D. Marzocca and H. Zhang, *Electroweak Higgs production with HiggsPO at NLO QCD*, *Eur. Phys. J. C* **77** (2017) 838 [[1710.04143](#)].
- [18] W. Astill, W. Bizoń, E. Re and G. Zanderighi, *NNLOPS accurate associated HZ production with $H \rightarrow b\bar{b}$ decay at NLO*, *JHEP* **11** (2018) 157 [[1804.08141](#)].
- [19] S. Alioli, A. Broggio, S. Kallweit, M.A. Lim and L. Rottoli, *Higgsstrahlung at NNLL'+NNLO matched to parton showers in GENEVA*, *Phys. Rev. D* **100** (2019) 096016 [[1909.02026](#)].
- [20] W. Bizoń, E. Re and G. Zanderighi, *NNLOPS description of the $H \rightarrow b\bar{b}$ decay with MiNLO*, *JHEP* **06** (2020) 006 [[1912.09982](#)].
- [21] S. Zanoli, M. Chiesa, E. Re, M. Wiesemann and G. Zanderighi, *Next-to-next-to-leading order event generation for VH production with $H \rightarrow b\bar{b}$ decay*, [[2112.04168](#)].
- [22] F. Granata, J.M. Lindert, C. Oleari and S. Pozzorini, *NLO QCD+EW predictions for HV and HV+jet production including parton-shower effects*, *JHEP* **09** (2017) 012 [[1706.03522](#)].
- [23] G.F. Giudice, C. Grojean, A. Pomarol and R. Rattazzi, *The Strongly-Interacting Light Higgs*, *JHEP* **06** (2007) 045 [[hep-ph/0703164](#)].
- [24] J. Elias-Miro, J.R. Espinosa, E. Masso and A. Pomarol, *Higgs windows to new physics through $d=6$ operators: constraints and one-loop anomalous dimensions*, *JHEP* **11** (2013) 066 [[1308.1879](#)].
- [25] G. D'Ambrosio, G.F. Giudice, G. Isidori and A. Strumia, *Minimal flavor violation: An Effective field theory approach*, *Nucl. Phys.* **B645** (2002) 155 [[hep-ph/0207036](#)].
- [26] C. Anastasiou, F. Herzog and A. Lazopoulos, *The fully differential decay rate of a Higgs boson to bottom-quarks at NNLO in QCD*, *JHEP* **03** (2012) 035 [[1110.2368](#)].
- [27] V. Del Duca, C. Duhr, G. Somogyi, F. Tramontano and Z. Trócsányi, *Higgs boson decay into b-quarks at NNLO accuracy*, *JHEP* **04** (2015) 036 [[1501.07226](#)].
- [28] F. Caola, K. Melnikov and R. Röntsch, *Analytic results for decays of color singlets to $g\bar{g}$ and $q\bar{q}$ final states at NNLO QCD with the nested soft-collinear subtraction scheme*, *Eur. Phys. J. C* **79** (2019) 1013 [[1907.05398](#)].
- [29] S.G. Gorishnii, A.L. Kataev and S.A. Larin, *The Width of Higgs Boson Decay Into Hadrons: Three Loop Corrections of Strong Interactions*, *Sov. J. Nucl. Phys.* **40** (1984) 329.

- [30] S.G. Gorishnii, A.L. Kataev, S.A. Larin and L.R. Surguladze, *Corrected Three Loop QCD Correction to the Correlator of the Quark Scalar Currents and $\Gamma_{\text{tot}}(H^0 \rightarrow \text{hadrons})$* , *Mod. Phys. Lett. A* **5** (1990) 2703.
- [31] S.G. Gorishnii, A.L. Kataev, S.A. Larin and L.R. Surguladze, *Scheme dependence of the next to next-to-leading QCD corrections to $\Gamma_{\text{tot}}(H^0 \rightarrow \text{hadrons})$ and the spurious QCD infrared fixed point*, *Phys. Rev. D* **43** (1991) 1633.
- [32] K.G. Chetyrkin, *Correlator of the quark scalar currents and $\Gamma_{\text{tot}}(H \rightarrow \text{hadrons})$ at $\mathcal{O}(\alpha_s^3)$ in p QCD*, *Phys. Lett. B* **390** (1997) 309 [[hep-ph/9608318](#)].
- [33] P.A. Baikov, K.G. Chetyrkin and J.H. Kühn, *Scalar correlator at $\mathcal{O}(\alpha_s^4)$, Higgs decay into b -quarks and bounds on the light quark masses*, *Phys. Rev. Lett.* **96** (2006) 012003 [[hep-ph/0511063](#)].
- [34] F. Herzog, B. Ruijl, T. Ueda, J.A.M. Vermaseren and A. Vogt, *On Higgs decays to hadrons and the R -ratio at N^4 LO*, *JHEP* **08** (2017) 113 [[1707.01044](#)].
- [35] R. Contino, M. Ghezzi, C. Grojean, M. Mühlleitner and M. Spira, *Effective Lagrangian for a light Higgs-like scalar*, *JHEP* **07** (2013) 035 [[1303.3876](#)].
- [36] R. Contino, M. Ghezzi, C. Grojean, M. Mühlleitner and M. Spira, *e HDECAY: an Implementation of the Higgs Effective Lagrangian into HDECAY*, *Comput. Phys. Commun.* **185** (2014) 3412 [[1403.3381](#)].
- [37] U. Haisch and G. Koole, *Beautiful and charming chromodipole moments*, *JHEP* **09** (2021) 133 [[2106.01289](#)].
- [38] A. Hayreter and G. Valencia, *Constraints on anomalous color dipole operators from Higgs boson production at the LHC*, *Phys. Rev. D* **88** (2013) 034033 [[1304.6976](#)].
- [39] J. Bramante, A. Delgado, L. Lehman and A. Martin, *Boosted Higgses from chromomagnetic b 's: $b\bar{b}h$ at high luminosity*, *Phys. Rev. D* **93** (2016) 053001 [[1410.3484](#)].
- [40] K.G. Chetyrkin and A. Kwiatkowski, *Second order QCD corrections to scalar and pseudoscalar Higgs decays into massive bottom quarks*, *Nucl. Phys. B* **461** (1996) 3 [[hep-ph/9505358](#)].
- [41] S.A. Larin, T. van Ritbergen and J.A.M. Vermaseren, *The Large top quark mass expansion for Higgs boson decays into bottom quarks and into gluons*, *Phys. Lett. B* **362** (1995) 134 [[hep-ph/9506465](#)].
- [42] W. Bernreuther, L. Chen and Z.-G. Si, *Differential decay rates of CP-even and CP-odd Higgs bosons to top and bottom quarks at NNLO QCD*, *JHEP* **07** (2018) 159 [[1805.06658](#)].
- [43] A. Behring and W. Bizoń, *Higgs decay into massive b -quarks at NNLO QCD in the nested soft-collinear subtraction scheme*, *JHEP* **01** (2020) 189 [[1911.11524](#)].
- [44] A. Behring, W. Bizoń, F. Caola, K. Melnikov and R. Röntsch, *Bottom quark mass effects in associated WH production with the $H \rightarrow b\bar{b}$ decay through NNLO QCD*, *Phys. Rev. D* **101** (2020) 114012 [[2003.08321](#)].
- [45] G. Somogyi and F. Tramontano, *Fully exclusive heavy quark-antiquark pair production from a colourless initial state at NNLO in QCD*, *JHEP* **11** (2020) 142 [[2007.15015](#)].
- [46] R. Akhouri, H. Wang and O.I. Yakovlev, *On the Resummation of large QCD logarithms in $H \rightarrow \gamma\gamma$ decay*, *Phys. Rev. D* **64** (2001) 113008 [[hep-ph/0102105](#)].

- [47] T. Liu and A.A. Penin, *High-Energy Limit of QCD beyond the Sudakov Approximation*, *Phys. Rev. Lett.* **119** (2017) 262001 [[1709.01092](#)].
- [48] Z.L. Liu and M. Neubert, *Factorization at subleading power and endpoint-divergent convolutions in $h \rightarrow \gamma\gamma$ decay*, *JHEP* **04** (2020) 033 [[1912.08818](#)].
- [49] J. Wang, *Resummation of double logarithms in loop-induced processes with effective field theory*, [[1912.09920](#)].
- [50] O. Brein, R. Harlander, M. Wiesemann and T. Zirke, *Top-Quark Mediated Effects in Hadronic Higgs-Strahlung*, *Eur. Phys. J. C* **72** (2012) 1868 [[1111.0761](#)].
- [51] K. Hamilton, P. Nason and G. Zanderighi, *MINLO: Multi-Scale Improved NLO*, *JHEP* **10** (2012) 155 [[1206.3572](#)].
- [52] K. Hamilton, P. Nason, C. Oleari and G. Zanderighi, *Merging $H/W/Z + 0$ and 1 jet at NLO with no merging scale: a path to parton shower + NNLO matching*, *JHEP* **05** (2013) 082 [[1212.4504](#)].
- [53] P. Nason, *A New method for combining NLO QCD with shower Monte Carlo algorithms*, *JHEP* **11** (2004) 040 [[hep-ph/0409146](#)].
- [54] S. Frixione, P. Nason and C. Oleari, *Matching NLO QCD computations with Parton Shower simulations: the POWHEG method*, *JHEP* **11** (2007) 070 [[0709.2092](#)].
- [55] S. Frixione, Z. Kunszt and A. Signer, *Three jet cross-sections to next-to-leading order*, *Nucl. Phys. B* **467** (1996) 399 [[hep-ph/9512328](#)].
- [56] S. Frixione, *A General approach to jet cross-sections in QCD*, *Nucl. Phys. B* **507** (1997) 295 [[hep-ph/9706545](#)].
- [57] S. Alioli, P. Nason, C. Oleari and E. Re, *A general framework for implementing NLO calculations in shower Monte Carlo programs: the POWHEG BOX*, *JHEP* **06** (2010) 043 [[1002.2581](#)].
- [58] PARTICLE DATA GROUP collaboration, *Review of Particle Physics*, *PTEP* **2020** (2020) 083C01.
- [59] R.D. Ball, V. Bertone, S. Carrazza et al., *Parton distributions from high-precision collider data*, *Eur. Phys. J. C* **77** (2017) 663 [[1706.00428](#)].
- [60] T. Sjöstrand, S. Ask, J.R. Christiansen, R. Corke, N. Desai, P. Ilten et al., *An introduction to PYTHIA 8.2*, *Comput. Phys. Commun.* **191** (2015) 159 [[1410.3012](#)].
- [61] P. Skands, S. Carrazza and J. Rojo, *Tuning PYTHIA 8.1: the Monash 2013 Tune*, *Eur. Phys. J. C* **74** (2014) 3024 [[1404.5630](#)].
- [62] J. Ellis, M. Madigan, K. Mimasu, V. Sanz and T. You, *Top, Higgs, Diboson and Electroweak Fit to the Standard Model Effective Field Theory*, *JHEP* **04** (2021) 279 [[2012.02779](#)].
- [63] ATLAS collaboration, *Measurements of the production cross-section for a Z boson in association with b-jets in proton-proton collisions at $\sqrt{s} = 13$ TeV with the ATLAS detector*, *JHEP* **07** (2020) 044 [[2003.11960](#)].
- [64] ATLAS collaboration, *Search for new resonances in mass distributions of jet pairs using 139 fb^{-1} of pp collisions at $\sqrt{s} = 13$ TeV with the ATLAS detector*, *JHEP* **03** (2020) 145 [[1910.08447](#)].
- [65] M. Cacciari, G.P. Salam and G. Soyez, *The anti- k_t jet clustering algorithm*, *JHEP* **04** (2008) 063 [[0802.1189](#)].

- [66] M. Cacciari, G.P. Salam and G. Soyez, *FastJet User Manual*, *Eur. Phys. J. C* **72** (2012) 1896 [[1111.6097](#)].
- [67] J.M. Butterworth, A.R. Davison, M. Rubin and G.P. Salam, *Jet substructure as a new Higgs search channel at the LHC*, *Phys. Rev. Lett.* **100** (2008) 242001 [[0802.2470](#)].
- [68] J.R. Andersen et al., *Les Houches 2015: Physics at TeV Colliders Standard Model Working Group Report*, in *9th Les Houches Workshop on Physics at TeV Colliders*, 5, 2016 [[1605.04692](#)].
- [69] N. Berger et al., *Simplified Template Cross Sections - Stage 1.1*, [[1906.02754](#)].
- [70] S. Amoroso et al., *Les Houches 2019: Physics at TeV Colliders: Standard Model Working Group Report*, in *11th Les Houches Workshop on Physics at TeV Colliders: PhysTeV Les Houches*, 3, 2020 [[2003.01700](#)].
- [71] ATLAS collaboration, *Measurement of VH , $H \rightarrow b\bar{b}$ production as a function of the vector-boson transverse momentum in 13 TeV pp collisions with the ATLAS detector*, *JHEP* **05** (2019) 141 [[1903.04618](#)].
- [72] ATLAS collaboration, *Measurements of WH and ZH production in the $H \rightarrow b\bar{b}$ decay channel in pp collisions at 13 TeV with the ATLAS detector*, *Eur. Phys. J. C* **81** (2021) 178 [[2007.02873](#)].
- [73] P.F. Monni, P. Nason, E. Re, M. Wiesemann and G. Zanderighi, *MiNNLO_{PS}: a new method to match NNLO QCD to parton showers*, *JHEP* **05** (2020) 143 [[1908.06987](#)].
- [74] P.F. Monni, E. Re and M. Wiesemann, *MiNNLO_{PS}: optimizing $2 \rightarrow 1$ hadronic processes*, *Eur. Phys. J. C* **80** (2020) 1075 [[2006.04133](#)].
- [75] G. Coloretti, A. Gehrmann-De Ridder and C.T. Preuss, *QCD Predictions for Event-Shape Distributions in Hadronic Higgs Decays*, [[2202.07333](#)].
- [76] *The POWHEG BOX*, <http://powhegbox.mib.infn.it>.
- [77] A. Alloul, N.D. Christensen, C. Degrande, C. Duhr and B. Fuks, *FeynRules 2.0 - A complete toolbox for tree-level phenomenology*, *Comput. Phys. Commun.* **185** (2014) 2250 [[1310.1921](#)].
- [78] T. Hahn, *Generating Feynman diagrams and amplitudes with FeynArts 3*, *Comput. Phys. Commun.* **140** (2001) 418 [[hep-ph/0012260](#)].
- [79] T. Hahn and M. Perez-Victoria, *Automatized one loop calculations in four-dimensions and D-dimensions*, *Comput. Phys. Commun.* **118** (1999) 153 [[hep-ph/9807565](#)].
- [80] T. Hahn, S. Paßehr and C. Schappacher, *FormCalc 9 and Extensions*, *PoS LL2016* (2016) 068 [[1604.04611](#)].
- [81] H.H. Patel, *Package-X: A Mathematica package for the analytic calculation of one-loop integrals*, *Comput. Phys. Commun.* **197** (2015) 276 [[1503.01469](#)].
- [82] R.N. Lee, *LiteRed 1.4: a powerful tool for reduction of multiloop integrals*, *J. Phys. Conf. Ser.* **523** (2014) 012059 [[1310.1145](#)].
- [83] S. Catani, *The Singular behavior of QCD amplitudes at two loop order*, *Phys. Lett. B* **427** (1998) 161 [[hep-ph/9802439](#)].
- [84] M. Misiak and M. Münz, *Two loop mixing of dimension five flavor changing operators*, *Phys. Lett. B* **344** (1995) 308 [[hep-ph/9409454](#)].

- [85] M. Gorbahn, U. Haisch and M. Misiak, *Three-loop mixing of dipole operators*, *Phys. Rev. Lett.* **95** (2005) 102004 [[hep-ph/0504194](#)].
- [86] CMS collaboration, *Measurement of differential cross sections for the production of top quark pairs and of additional jets in lepton+jets events from pp collisions at $\sqrt{s} = 13$ TeV*, *Phys. Rev. D* **97** (2018) 112003 [[1803.08856](#)].
- [87] M. Czakon, D. Heymes, A. Mitov, D. Pagani, I. Tsinikos and M. Zaro, *Top-pair production at the LHC through NNLO QCD and NLO EW*, *JHEP* **10** (2017) 186 [[1705.04105](#)].
- [88] F. Krauss, S. Kuttimalai and T. Plehn, *LHC multijet events as a probe for anomalous dimension-six gluon interactions*, *Phys. Rev. D* **95** (2017) 035024 [[1611.00767](#)].
- [89] V. Hirschi, F. Maltoni, I. Tsinikos and E. Vryonidou, *Constraining anomalous gluon self-interactions at the LHC: a reappraisal*, *JHEP* **07** (2018) 093 [[1806.04696](#)].
- [90] R. Goldouzian and M.D. Hildreth, *LHC dijet angular distributions as a probe for the dimension-six triple gluon vertex*, *Phys. Lett. B* **811** (2020) 135889 [[2001.02736](#)].
- [91] O. Brein, R.V. Harlander and T.J.E. Zirke, *vh@nnlo - Higgs Strahlung at hadron colliders*, *Comput. Phys. Commun.* **184** (2013) 998 [[1210.5347](#)].
- [92] R.V. Harlander, J. Klappert, S. Liebler and L. Simon, *vh@nnlo-v2: New physics in Higgs Strahlung*, *JHEP* **05** (2018) 089 [[1802.04817](#)].